Mustaf Raif Bekteshi

Mechanical and optical characterisation of glass optical fibres for sensing applications

Mechanical and optical characterisation of glass optical fibres for sensing applications

By

Mustaf Raif Bekteshi

THE UNIVERSITY of ADELAIDE

A thesis submitted of the degree of

Master of Philosophy

in the

Faculty of Sciences

School of Chemistry & Physics

May 2019

Contents

LIST OF FIGURES

LIST OF TABLES

PUBLICATION

Conference papers

E. P. Schartner, G. Tsiminis, M. Bekteshi, H. Ebendorff-Heidepriem, “Improved fabrication techniques of extruded simplified hollow core optical fibres for Raman spectroscopy”. Proc. Optical Fibres and Sensors, San Franciscio, U.S.A. (2018)

G. Tsimins, E. P Schartner, M. Bekteshi, M.R. Hutchison, H. Ebendorff-Heidepriem, “Hollow-core fibres made by glass billet extrusion as sensor for Raman spectroscopy”. ACOFT, Sydney, Australia (2016)

ABSTRACT

The capacity of glass optical fibres to handle stress experienced in sensing application is critical in many areas including biomedical sensing. Accordingly, it is important to determine the tensile strength of optical fibre, providing better understanding of optical fibre strength and the behaviour of optical fibre under certain stresses. This thesis covers the mechanical and optical characterisation of a range of solid glass optical fibres, including solid fibres made of various glass materials, stored lead silicate solid fibre and microstructured optical fibre made of silica glass material.

This thesis employs standard mechanical testing techniques such as tensile testing. Data collected from the tensile strength tests is used to understand the statistical behaviour of solid fibres and characterise them mechanically using the statistical Weibull distribution technique. In addition, the strength of numerous solid glass optical fibres made of different glass materials are compared.

Firstly, data indicates that depending on the glass material, the strength of the fibre under tensile load varies from very high strength for standard telecommunication fibre, such as solid SMF28, to very low strength for ZBLAN fluoride glass fibres.

Secondly, using the same statistical technique for data analysis, an investigation of the effect of aging (storage time) in F2 solid glass fibre was carried out. Results indicate that the aging effect does not have significant effect on the strength of solid F2 glass fibres.

Additionally, an investigation was undertaken into the effect of capillary hole size (inflation ratio) and presence of multiple holes on the strength of microstructured glass optical fibres. Results indicate that the inflation ratio and presence of multiple holes in the fibre affects the strength of the fibre.

This thesis presents an investigation of the optical characterisation of solid and hollow core optical fibres. Raman spectroscopy of the glass materials was also conducted to explore their potential application in biomedical sensing.

DECLARATION

I certify that this work contains no material which has been accepted for the award of any other degree or diploma in my name, in any university or other tertiary institution and, to the best of my knowledge and belief, contains no material previously published or written by another person, except where due reference has been made in the text. In addition, I certify that no part of this work will, in the future, be used in a submission in my name, for any other degree or diploma in any university or other tertiary institution without the prior approval of the University of Adelaide and where applicable, any partner institution responsible for the joint-award of this degree.

I give permission for the digital version of my thesis to be made available on the web, via the University's digital research repository, the Library Search and also through web search engines, unless permission has been granted by the University to restrict access for a period of time.

I acknowledge the support I have received for my research through the provision of an Australian Government Research Training Program Scholarship.

Adelaide, May 2019

_____

Mustaf Raif Bekteshi

ACKNOWLEDGMENTS

It is my great pleasure to thank all the people who made this thesis possible. First, I would like to sincerely thank my wonderful supervisors, Prof. Heike Ebendorff-Heidepriem, Dr. Erik Schartner, and Dr. Georgios Tsiminis. A special thank you goes to Heike for making this research realizable by setting up a great working environment at IPAS. Your passion for science and work ethic has driven me to become the person I am today. By setting achievable goals you helped me accept more responsibility in my life journey. Working under your supervision allowed me to gain more confidence, and with your support to gain a foothold in the optical production industry. For all this and more, I will never be able to repay you for your guidance.

Many thanks to the supporting cast, Erik and Georgios for all the support you provided throughout this time. Helping me to stay on the right path even when it was somewhat windy and foggy. I sincerely wish you deep success and happiness in your own personal journeys in the research world.

I would also like to thank Milad Abou Dakka for his help proof reading and finalizing my thesis, and for the many days we spent discussing problems I faced during this project. You truly inspired me and left a great impact on me, as I learned from you how to remain resilient during hard times.

I also would like to thank Alson Ng, Alastair Dowler, and Anthony Leggatt for their technical support.

And last, but with all my sincerity and my heart I would like to thank my darling wife Egzona. Your unconditional support encourages me to stay focused on my work without worrying about uncertainties of the future. I still don't know how you managed to put up with me during this most stressful period of our lives. You are a great example of a strong woman who can simultaneously raise and educate children while supporting an ambitious husband. To thank you adequately, words are not enough. I don't think you will ever know what your support, understanding and encouragement over these past 10 years of our life together has meant to me. Here's to a beautiful future together.

SUMMARY

This thesis covers work related to the mechanical and optical characterisation of both solid and air hole glass optical fibres made of different glass materials. This work can be applied to optical fibre research and help to optimise the fabrication procedure of glass fibre made of silica glass as well as fibres made of soft glass.

Chapter 1 introduces the work of this thesis and briefly describes the techniques used for mechanical and optical characterisation. Glass materials that are used for fibre fabrication for applications in biomedical sensing are introduced. Additionally, a brief description is provided of the fibre types tested in this work.

Chapter 2 reviews the literature on optical fibres and the basic laws that describe the optical properties of the step index optical fibre. It also covers the fabrication process used for microstructured fibre fabrication, including their light guiding mechanism.

Chapter 3 reviews the literature on the mechanical properties of glass optical fibres subjected to a pulling – or tensile – force. A review of the literature on the statistical behaviour of solid glass optical fibre failure is also provided. The most common statistical distribution used to model this behaviour, known as the Weibull distribution, is described.

Chapter 4 documents the experimental work conducted on the mechanical characterization of solid glass optical fibres during this Master's project. This begins with an introduction of the glasses that is used for fibre fabrication. Here, the Weibull distribution is employed to characterise the behaviour of different glass fibre materials such as commercial silica of different grades (LWQ, F300), technical borosilicate glass (Duran), commercial lead-silicate glass (F2), in-house made germanate (Ge), tellurite (Te) and fluoride (ZBLAN) glasses in comparison with standard step index fibre SMF28 with cladding made of F300 glass. The effect of storage (stored time) on uncoated F2 solid fibre is measured and characterised using the Webull distribution. Additionaly, the same statistical model is used to characterise the behaviour of suspended core optical fibre (SCF which contain three holes) and capillary fibre which contain a single hole .

Chapter 5 examines optical properties such as fibre loss and the background Raman spectra of the glass materials that are of interest for making fibre for Raman based sensors. The fibre loss and background Raman spectra are critical considerations as Raman signals are typically weak, and these two factors can reduce the ability to extract the Raman signal of a measured sample. The loss measurements are conducted in solid glass fibre made of Duran and solid glass fibre made of F2. Loss measurements of hollow core optical fibres made of F2 glass are also included.

Chapter 6 summarises the results presented in earlier chapters, and discusses the conclusions derived from these results. Future work is suggested based on the lessons learned in this work as well as the possible future pathways this research could take.

Background of Mechanical and Optical Characterisation of Glass Optical Fibres

Chapter 1 – Introduction

Historically, optical fibres were predominantly applied in the telecommunications field [1]. In addition to these traditional applications, use of fibres within the field of biomedical sensing is growing rapidly from advances in technology within the field [2-4]. Optical fibres play a major role in techniques for imaging and other diagnostic procedures, [5] as they can provide access to otherwise inaccessible parts of the body [6]. In addition, optical fibres can also be used for optical sensing purposes such as detecting chemical components in biological and chemical solutions [7]. In general, knowing the tensile strength of optical fibre is a key component since optical fibre can degrade to the point of catastrophic failure during service resulting in loss of signal transmission and potential damage to the sample itself [8].

Many of the environments in which optical fibres are used can cause stresses to the fibre, leading to mechanical damage [9]. For instance, these devices are often used in spaces with milimetric, or even microscopic, dimensions, such as blood vessels or other parts of the body [6, 10], where fibres can easily be pulled and bent, which could lead to fibre failure. Optical fibres with applications in biosensing are also subjected to various stresses from use and handling [5]. Other sensing applications where tensile strength measurements are important include chemical sensing, sensing in the construction and aircraft industry where sensors can often be exposed to high stresses. Therefore strength and reliability of optical fibres must be characterised [11, 12]. To this end, the method that is most commonly used to determine the strength of the optical fibre is the so-called Weibull distribution [13], a statistical method used to quantify the behaviour of glass optical fibre subjected to various stresses.

Fibre strength is strongly dependent on the choice of glass materials, as different materials differ in mechanical properties [14]. Pure silica glass consisting of pure SiO_2 is desirable due to its high mechanical strength [7]. One way to change the properties of pure silica glass can be achieved by adding different materials with pure silica that affect, amongst other things, the melting point of the resulting glass. Based on this, these compound glasses can be separated in two categories. The first one is hard glass: for example, borosilicate glass such as Duran or BK7 possessing high softening temperature and high mechanical strength leading to hard glass. The second one is soft glass such as lead silicate (F2), germanate, fluoride (ZBLAN), and tellurite glass, have lower softening temperatures compared to pure silica glass and also compare to hard glass, which makes them more suitable for techniques such as fibre preform extrusion [4, 15, 16]. However, the lower softening temperature correlates in general with low mechanical strengths which is undesired.

Optical fibres can be classified based on the type of ***glass materials*** used to fabricate the fibres. Silica fibre, for instance, is one of the most widely used optical fibre material in the fields

of telecommunication and sensing. Other types of optical fibre glass materials include those made of soft glass, some of which are mentioned above. Generally, for different transmission window, different materials are suitable [17]. Also, soft glass fibres have higher refractive index than silica fibre, and some soft glass types such as fluoride and chalcogenide have better transmission than silica fibre in the infrared (IR) (longer than 2.5 μm) [18].

Fibres can also be classified based on their ***structures***. The most common optical fibres are known as step-index optical fibres where the entire cross-section of the fibre is solid but with a uniform refractive index of the material throughout the core [19] There is also a growing interest in microstructured optical fibres (MOFs), which are made by integrating holes along the length of the optical fibre [14]. Since the introduction of MOFs, their development has expanded and resulted in different types of MOFs such as suspended core optical fibres (SCFs) and hollow core optical fibres (HCFs) [17, 20, 21].

This thesis focuses on understanding and characterising optical fibres in terms of their mechanical strength, examining the effects of the glass material, their inner structural geometry, and aging. Understanding of these parameters enables a balanced selection between mechanical and optical characteristics. Therefore, the theory as well as the methods used to measure the tensile strength of optical fibres is discussed. In this study, fibre glass materials and structures are explored for mechanical testing of optical fibre-based sensors. The following studies are conducted:

- Comparison of different glass fibre materials listed in Table 1.
- Comparison of aged (stored) F2 glass fibre with non aged F2 glass fibre.
- Comparison of suspended core optical fibre (SCF) with capillary fibre (one hole) and solid optical fibre.

As these fibres are aimed at sensing applications, this work also includes also a brief examination of optical properties was carried out such as fibre loss of a few fibres made at the Institute for Photonic and Advanced Sensing (IPAS) as well as bulk glass Raman signal.

Chapter 2 – Background: Optical Properties of Glass Optical Fibres and Fabrication Process of Microstructured Glass Optical Fibres

2.1 – Optical fibre

An optical fibre is a cylindric dielectric waveguide that transmits electromagnetic energy within the optical spectrum. The thickness of an optical fibre is comparable with that of a human hair. Typically, optical fibres are made from three parts, as shown in Figure 1; the core, which is the central part of the fibre where light is confined, the cladding, which surrounds the core, and the outer protective coating (or jacket), which protects the inner parts of the fibre [19, 22].

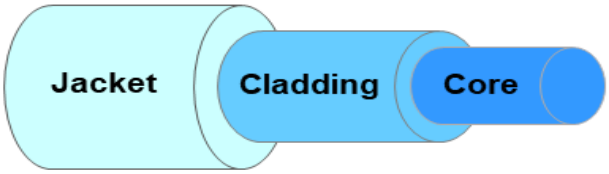

Figure 1. Schematic of optical fibre used in telecommunication.

Light in optical fibres propagates on the principle of total internal reflection (TIR). When light crosses from one medium to another whereupon the refractive index (RI) changes, the light partially reflects and refracts, as shown in Figure 2. As the incident beam travels from the medium with higher RI n_{cr} (refractive index of core n_{cr}) into the medium with lower RI n_{cl}(refractive index of cladding n_{cl}), the transmitted part refracts away from the normal at the interface boundary. Considering a light beam traveling n_{cr} to n_{cl} (recalling that n_{cr}> n_{cl}), the light crossing the interface boundary is deviated away from the normal. In the case where the incident angle θi results in transmitted light travelling along the interface with transmitted angle $\theta t = 90^0$, this incident angle is known as the critical angle θc. This behavior is captured by Snell's law [23]:

$$n_{cr} \sin \theta_i = n_{cl} \sin \theta_t. \qquad 2.1$$

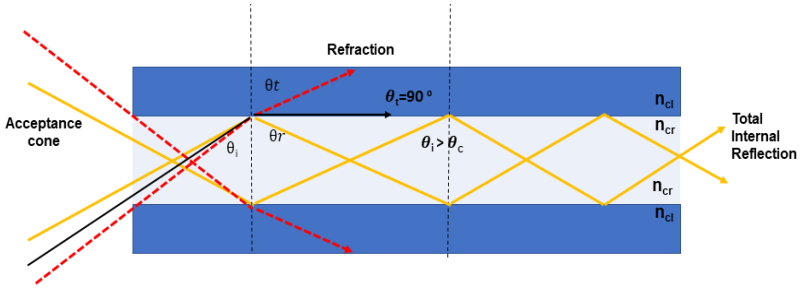

Figure 2. Reflection and refraction of incident light at medium interface. TIR occurs at incident angles greater than the critical angle, $\boldsymbol{\theta c}$. Incident light represent the direction of wave propagation.

For incident light at an angle greater than the so-called critical angle, light is reflected as shown in Figure 2. This phenomenon is known as total internal reflection. The critical angle can be found by substituting 90^0 into Equation 2.1 for the transmitted angle [17, 22-24]:

$$\theta_c = \arcsin\left(\frac{n_{cl}}{n_{cr}}\right) \quad 2.2$$

Light is coupled into the fibre when it is incident at an angle below that required for TIR once inside the fibre; this angle θ_{max},is defined as the half angle of the acceptance cone of the fibre. The θ_{max} is related to the numerical aperture (NA) and the refractive index of the outside medium (n_a) by the following expression:

$$NA = n_a \sin\theta_{max} = \sqrt{n_{cr}^2 - n_{cl}^2} \quad 2.3$$

Light can be guided through the fibre at many different angles $\theta_i > \theta_c$, resulting in multiple guiding pathways that give rise to multiple optical modes of propagation within the fibres. An optical fibre is defined as single mode or multimode by its core size, numerical aperture (NA), and the operating wavelength of propagating light, and is represented by:

$$V = NA\frac{2\pi}{\lambda}d_c. \quad 2.4$$

V is the so-called V- number that (when $n_{cr} \approx n_{cl}$) for single mode is $V < 2.405$ and for multi-mode is $V > 2.405$, λ is the wavelength of light and NA is the numerical aperture of the optical fibre which is defined in Equation 2.3. Based on this, the fibre is said to be either single mode (SMF) or multi-mode (MMF).

2.1.1 – Transmission loss

In optical fibres there are two loss mechanisms; interfacial and transmission losses. The interfacial loss including both Fresnel reflections and coupling losses. The interfacial loss is not covered in cutback loss measurement, while coupling losses can be minimized with optimised coupling into the fibre, therefore such losses will not be discussed further in this thesis. Transmission loss refers to losses that occur along the length of the fibre. As for transmission loss, the amount of light lost between input and output of the optical fibre is known as attenuation. In general, the transmission loss in an optical fibre is expressed as the sum of all losses. Transmission loss within the optical fibre is represented by [25, 26]:

$$\alpha = \frac{10}{L}log\frac{P_i}{P_o}, \quad 2.5$$

where P_i is the input power, P_o is output power and L is the length of propagation. There are a number of components which can influence the overall transmission loss while light propagates through the core, such as core surface, core/cladding interface , material absorption, waveguide

losses and water absorption [17, 22-25]. Another component which contributes to transmission loss is confinement loss due to leakage nature of the mode, and geometry deformation of the fibre structure that can occur during the fibre fabrication process, which plays a major role in MOFs [27]. Figure 3 shows the spectral attenuation in silica as is used in telecommunication [28]. This loss spectrum shape particularly at UV and near IR depends on the glass material used in the optical fibre [17, 22-25].

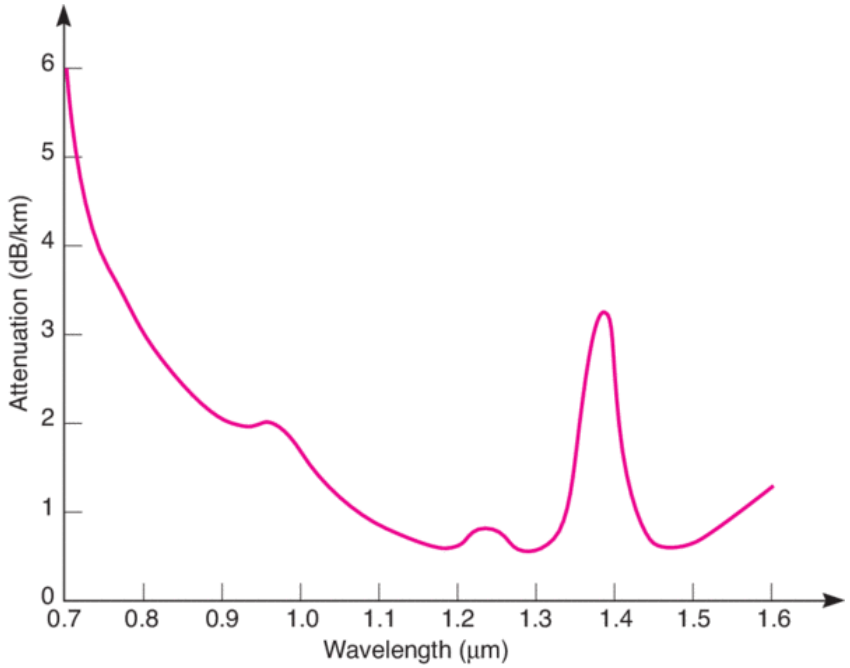

Figure 3. Loss of a standard telecommunication fibre due to wavelength [28].

The transmission loss applies to all fibres. Therefore, Equation 2.5 is used in optical characterisation, and specifically in optical fibre loss measurements. In the following section, we review MOF characteristics in greater detail.

2.2 – Microstructured optical fibre (MOF)

MOFs are a type of fibre made by integrating holes along the optical fibre which can have a variety of geometries, some of which are shown in Figure 4. The structures in MOFs provide the waveguide mechanism, so that MOF optical properties are determined by their inner structural geometry [29].

There are different types of MOF including the suspended core fiber (SCF) shown in Figure 4a, where light is guided based on TIR [24, 30] and demonstrates great performance in sensing such as dip sensing for detection of small sample volumes of chemicals or biomolecules [4]. Another type of MOF is the hollow core fibre (HCF), which is a type of optical fibre where light is guided in a hollow air core instead of a solid glass core (Figure 4b). There are two common light guidance mechanism in HCF, the photonic band gap guidance [30] and antiresonance guidance [31,

32].The internal structure determines the optical properties of the fibre by guiding light in the hollow core surrounded by microstructure cladding and a solid outer jacket for mechanical stability, making HCF an attractive approach for efficient biomedical sensor designs [14].

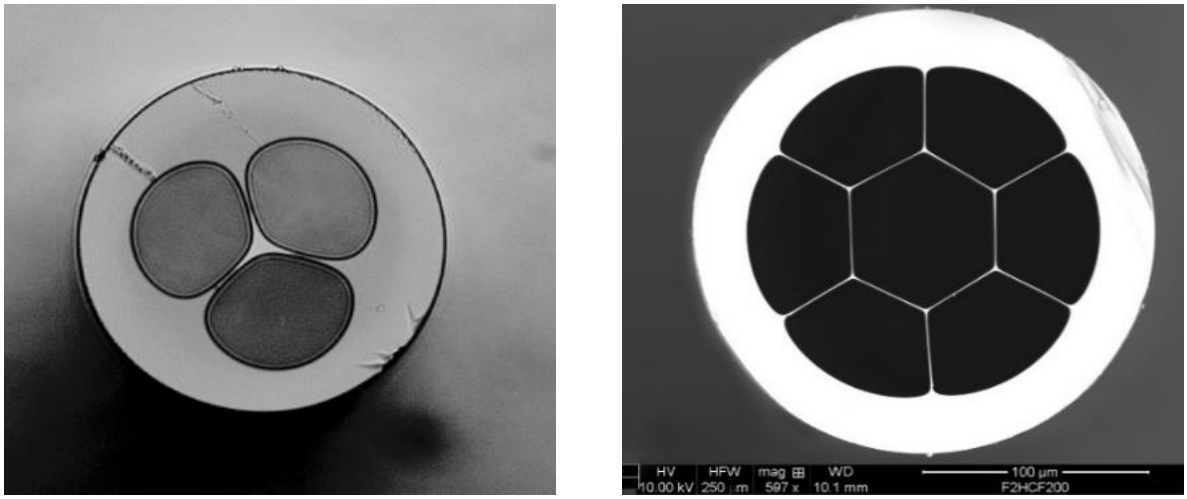

a *b*

Figure 4. Cross–sectional image of MOF a) Suspended core optical fibre, b) HCF with hexagonal inner structure [33].

2.2.1 – Fabrication Process of MOF

The fabrication method of the optical fibre preform can be different for different types of optical fibre. For instance, the fabrication method of the preform of the standard telecommunication single mode optical fibre (SMF) from which fibre is drawn, is made by a process known as chemical vapor deposition (CVD) [34]. The MOF fabrication is a complex process that requires multiple fabrication steps. The most important part of making a MOF is the fabrication of the preform of the MOF from which the fibre is drawn. A variety of techniques and glass materials have been used to date [35, 36]. The most widely used method to fabricate MOF preforms is capillary stacking. Capillary stacking is a technique where capillary tubes are stacked together in a hexagonal structure to make the preform. This technique gives flexibility in terms choosing location of the core. However, fabricating a fibre preform using capillary stacking technique is labor-intensive [36, 37]. There are other methods that can be employed in fabrication of the MOFs preforms such as milling, which was used to make the SCFs tested in this thesis [38]. Another method to make MOF preforms is the glass billet extrusion technique, which is a technique where a glass billet is heated up to its softening point and then forced through a structured metal opening known as a die. The inner holes, wall size and their arrangement in preform are determined by the die exit geometry [14, 39]. This fabrication technique amongst other techniques enables the production of a preform with a wide range of inner structural geometry [3, 14, 33, 35], therefore

the glass billet extrusion is predicted to be an appropriate technique for HCFs and is suitable for soft glass. The glass billet extrusion technique was used to make HCFs, for which loss measurements was performed (see Chapter 5).

Chapter 3 – Mechanical Properties, Fracture Mechanism, and Failure Weibull Distribution of Glass Optical fibre

3.1 – Mechanical properties (Hooke's Law)

When optical fibres are subjected to pulling forces, they initially show an elastic deformation and eventually they fail at some value of force. In this section we will study this effect, separating it into the elastic regime and the failure regime [1]:

$$K = \frac{|F|}{|\Delta L|}, \qquad 3.1$$

where K is the elasticity constant, ΔL is the absolute elongation introduced by pulling force F. The relative elongation (the measured parameter in this study) is the ratio of absolute elongation to the initial length of fibre under pulling force and is given by:

$$\varepsilon = \frac{\Delta L}{L_0}, \qquad 3.2$$

where Lo is the initial length of the fibre. Combining equations 3.1 and 3.2, the elasticity constant of the fibre can be given by:

$$K = \frac{F}{\varepsilon L_0}, \qquad 3.3$$

According to Equation 3.3, the optical fibre elasticity constant is represented by the linear fitting of the force as a function of relative elongation divided by the initial fibre length.

The stress of a uniaxial tensile loading of the fibre is related to the magnitude of its cross-sectional area as follows:

$$\sigma = \frac{F}{A}, \qquad 3.4$$

where F is the applied force, A is the cross-sectional area of the optical fibre and σ is the pulling stress. The linear relationship of the pulling stress and the fibre relative elongation gives the slope which represents the Young's modulus shown in Equation 3.5, which also is the slope of force as a function of elongation, with the limit that highest force is the force at failure, i.e. highest elongation that can be achieved is the elongation at failure.

$$E = \frac{\sigma}{\varepsilon} = \frac{KL_0}{A}, \qquad 3.5$$

and is a measure of the ability of a material to withstand deformation under tensile or compressive stress [1, 40, 41].

3.2 – Fracture mechanism: Linear Elastic Fracture Mechanism

The mechanical behavior of the optical fibre is modelled by linear elastic fracture mechanism (LEFM) theory, which is suitable for linear elastic and brittle materials such as optical fibres. LEFM theory assumes that elastic and brittle materials of a certain geometry under linear stress fail due to the presence of defects (cracks); the two important parameters therefore are crack size and geometry. Cracks are modelled as defects with defined geometry and lying in a particular plane. They can be located on the fibre surface or embedded within the material itself. Three types of crack formations are considered: type **I** which is crack opening (or widening), type **II** is in-plane crack sliding (or in-plane shearing), and type **III** is anti-plane crack sliding (anti-plane shearing). These types are distinguished by the direction of the force, which can be parallel or perpendicular to the plane of the crack. Based on fundamental work, Irwin and others [42] developed the concept of the stress intensity factor. The glass failure rule can be expressed in simple terms: "the material fails if the stress intensity factor K_I due to tensile stress at the tip of one crack reaches its critical value K_{IC} "[42]. The Irwin equation for fracture in LEFM form is given by:

$$K_{IC} = \sigma_f \beta \sqrt{a_c}, \qquad 3.6$$

where K_{IC} is a material constant known as the fracture toughness (for fused silica glass K_{IC} = 0.75 MPa.m $^{1/2}$ [43]), σ_f is the fracture stress of the fibre (stress at which failure occurs known as stress at failure), a_c is the critical crack size, and β is a dimensionless geometrical term that depends on the crack and loading geometries: e.g. for a semicircular crack in the surface of the fibre assuming a plane stress hypothesis and a tensile loading case β = 1.16 [40]. Due to the brittle nature of glass optical fibres, for which rupture is due to the catastrophic propagation of cracks initiated at defect sites, the measured values are distributed and, hence, require a statistical treatment [42].

3.2.1 – Strength of the glass optical fibre

The strength of an optical fibre is a key component in the reliability of a fibre, since it can degrade to the point where failure could occur during service which could lead to complete loss of signal transmission [8] and potential damage to the sample itself. The optical fibre strength (stress at failure) is determined by defect size, and location [44]. Also, at temperatures below the glass transition temperature, T_g, glass is brittle, and its failure is stochastic [45].The theoretical strength of a glass material, σ_{th}, depends on the glass properties and can be described by the following expression [40, 45]:

$$\sigma_{th} = \sqrt{\frac{E\zeta}{r_0}}, \qquad 3.7$$

where *E* is Young's modulus, ζ is the surface energy and r_0 is the atomic bond length (Si-O). For example the theoretical strength (σ_{th}) for silica glass is 16 GPa, which is much higher than its experimentally measured value (0.69 GPa). [45]. This huge discrepancy is attributed to the defects along the glass fibre surface [46]. There are two main types of defects related to fibre failure; extrinsic and intrinsic defects.

Extrinsic defects originate mainly from outside factors, those defects are introduced mainly to the surface during contact of the fibre with any hard surface for example spooling the fibre on a drum [47]. Other extrinsic defects can be caused by handling during tensile measurements such as stripping off the coating, placing the fibre in aluminium plates, and gluing. Additionally, the strength degradation of the optical fibre can be caused by the interaction of the fibre with humid environments, in which fibres are stored [44]. Over time, glass fibres degrade due to defects caused by surface scratches and moisture [1, 8, 48, 49] , which is why they are usually protected by one or multiple protective coating layers [49].These defects can lead to fibre strength degradation and to failure for low applied stress known as early stress at failure [43].

Intrinsic defects stem from inner defects originating mainly from glass quality and fibre drawing condition such as drawing temperature, susceptor, drawing speed and other drawing parameters. If a fibre contains only intrinsic defects, this could lead to failure at larger applied stresses [50].

To ensure the reliability of an optical fibre, it is necessary to determine the strength of the optical fibre. Hence, to characterise a fibre's mechanical behaviour, it is necessary to determine two parameters:

a) strength (the stress where failure occurs),
b) strength distribution [43].

To determine the above parameters, a technique is employed called uniaxial tensile loading or tensile strength measurement technique shown in experimental part of this thesis. This technique is very common and simple; the ends of the fibre are pulled in opposite directions, where the stress (pulling stress) is assumed to be distributed uniformly over the fibre surface [40, 43, 45]. Thus, the failure probability depends on the load to which the glass is subjected.

3.3 – Stress to failure statistical analyses: Weibull Distribution

The flaws or defects in the fibre surface cause the strength of the fibre to vary considerably between samples, no matter which technique is used to break the fibre. Since glass is a brittle material and its strength can vary drastically even between lengths of the same fibre, analysis of the strength of an optical fibre is most commonly done using the Weibull distribution, a statistical method to determine the reliability of materials [48]. This type of method is found to be used in many statistical analyses of the strength of materials due to its suitability even for small numbers

of the tested samples [36, 51].The most common form of the Weibull distribution used in literature is the two-parameter (unimodal) Weibull distribution [40]. The linearized form of this Weibull distribution is:

$$Ln\left(Ln\left(\frac{1}{1-P}\right)\right) = m\,Ln\,\sigma - m\,Ln\,\sigma_0, \qquad 3.8$$

where P is the probability of failure, σ is the tensile stress at failure, m is the Weibull slope which represents the defect size distribution (defect size variation), i.e. a high value of m indicates that the size of defects on the fibre surface is narrowly distributed, resulting in narrow failure distribution. Conversely, a low value of m indicates that the size of defects along the fibre surface is broadly distributed, leading to cracks of largely varying sizes between samples. This in turn leads to more scattered values of stress at failure between fibre samples [50, 51]. And σ_0 is a scale parameter known as the characteristic strength (strength at which 63.2% of failures occur). The characteristic strength σ_0 is conventionally chosen to be 63.2% as this is the value at which the reliability is $1\text{-}e^{-1}$ [52]. Therefore, the Weibull distribution provides a relationship between the probability of failure, *P*, of an optical fibre with stress at failure to which the fibres are subjected. An estimate of the failure probability can be obtained using median rank approximation as follows [36]:

$$P = \frac{i-0.3}{N+0.4}, \qquad 3.9$$

where i is the order of each fibre sample according to the stress at failure in ascending order, N is the total number of the fibre sample in the population.

When the probability failure versus stress at failure of the fibres, plotted as a linearized Weibull distribution, does not fall on a straight line but instead in a curved line, a third parameter in the Weibull distribution can be used to straighten the curved distribution data. This parameter is called the location parameter γ, see Equation 3.10 below:

$$\mathrm{Ln}\left(\mathrm{Ln}\left(\frac{1}{1-\mathrm{P}}\right)\right) = \mathrm{m\,Ln}(\sigma-\gamma) - \mathrm{m\,Ln}\,\sigma_0, \qquad 3.10$$

and this kind of Weibull distribution is known as a three-parameter Weibull distribution [51, 53]. However, in this thesis the failure populations contain multiple curves, likely caused by the various defects mentioned, and as such the measured values could be better explained with a bimodal two-parameter function than with a third-parameter function.

Experimental results

Chapter 4 – Tensile Strength Measurements and Stress to Failure Analysis of Optical Fibres Made of Various Glass Materials

4.1 – Glass optical fibres type

This section discusses solid fibres made of different glass types, and fibres with air holes made of two types of silica. Table 1 summarises information regarding fibre structure, glass type, fabrication technique and the fibre dimensions such as inner diameter (ID) and outer dimeter (OD). Fibres are compared to a reference fibre (standard, commercially available SMF28 named as SMF28(F300) due to the cladding made of F300 glass material) with well-known strength.

In this thesis, fibres that are tested are made of different glass materials such as:

- F300 which is fused silica, for production of which chemical precursors ($SiCl_4$) are used,
- LWQ which is quartz silica, for production of which raw material such as quartz sand or quartz crystal are used,
- Duran borosilicate glass,
- F2 lead-silicate glass,
- Ge germanate glass,
- Te tellurite glass,
- ZBLAN fluoride glass.

The types of the fibres tested here are:

- Solid fibre such as:
  - SMF28(F300), commercially available,
  - LWQ, drawn in-house from commercial rod preforms,
  - Duran, drawn in-house from commercial rod preforms,
  - F2 (labelled here as F2a, F2b, F2c, and F2d due to different fabrication dates), drawn from in-house extruded rods that were made from commercial billets,
  - Ge, made from in-house extruded rods that were made from in-house fabricated glass billets,
  - Te, were made from in-house extruded rods that were made from in-house fabricated glass billets,
  - ZBLAN, were made from in-house extruded rods that were made from in-house fabricated glass billets.
- F300 capillary fibre drawn in-house from commercial tube preform,
- F300 SCF fibre drawn in-house from in-house milled preform made from commercial rod.
- LWQ SCF fibre drawn in-house from in-house milled preform made from commercial rod.

Table 1. The glass optical fibre types, their dimesions and their fabrication technique.

Fibre structure	Glass material type	Code	OD (um)	ID (um)	Fabrication technique
Solid fibre	Fused Silica	SMF28(F300)	125		Commercially avalable, made of F300
	Quartz Silica	LWQ	125		Drawn into fibre from commercial rod
	Borosilicate	Duran	160		Drawn into fibre from commercial rod
	Lead silicate	F2a	160		Drawn into fibre from commerical rod
	Lead silicate	F2b	160		Drawn into fibre from extruded rod preform made of commercial rod
	Lead silicate	F2c	160		Drawn into fibre from extruded rod preform made of commercial rod
	Lead silicate	F2d	160		Drawn into fibre from extruded rod preform made of commercial rod
	Germanate	Ge	160		Drawn into fibre from extruded rod preform
	Tellurite	Te	160		Drawn into fibre from extruded rod preform
	Fluoride	ZBLAN	160		Drawn into fibre from extruded rod preform
Suspended core (three hole)	Quarzt Silica	LWQ-SCF	160		Drawn into fibre from in-house preform made from commercial rod
	Fused Silica	F300-SCF	160		Drawn into fibre from in-house preform made from commercial rod
Capillary (single hole)	Fused Silica	F300-C1	125	36	Drawn into fibre from commercial capillary preform
	Fused Silica	F300-C2	125	40	Drawn into fibre from commercial capillary preform
	Fused Silica	F300-C3	125	56	Drawn into fibre from commercial capillary preform
	Fused Silica	F300-C4	125	66	Drawn into fibre from commercial capillary preform
	Fused Silica	F300-C5	125	75	Drawn into fibre from commercial capillary preform

4.2 – Experimental method of uniaxial tensile test

To determine the stress at failure of the optical fibre the uniaxial tensile test is employed. A 150mm linear translation stage stepper motor is used to conduct the tensile measurements.

Individual fibres of a length of 100 mm are mounted onto an aluminium plate by gluing the end of the fibre using Loctite® 406 instant adhesive (>80% ethyl cyanoacrylate), which is kept for 15 minutes (sufficent for the fibre to dry). This apparatus is shown in Figure 5. To avoid slipping of the aluminium plates on which the fibre is glued, the plates are placed on to the stages with lips (bath shape). Simultaneously, aluminium plates are clamped onto the stages to avoid any tripping of the plates from the stage lips as shown in Figure 6.

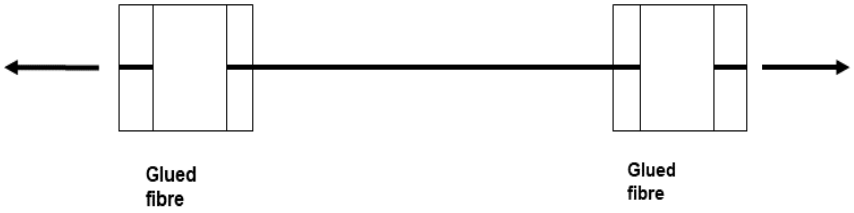

Figure 5. Schematic of the fibre attached to the aluminium plate.

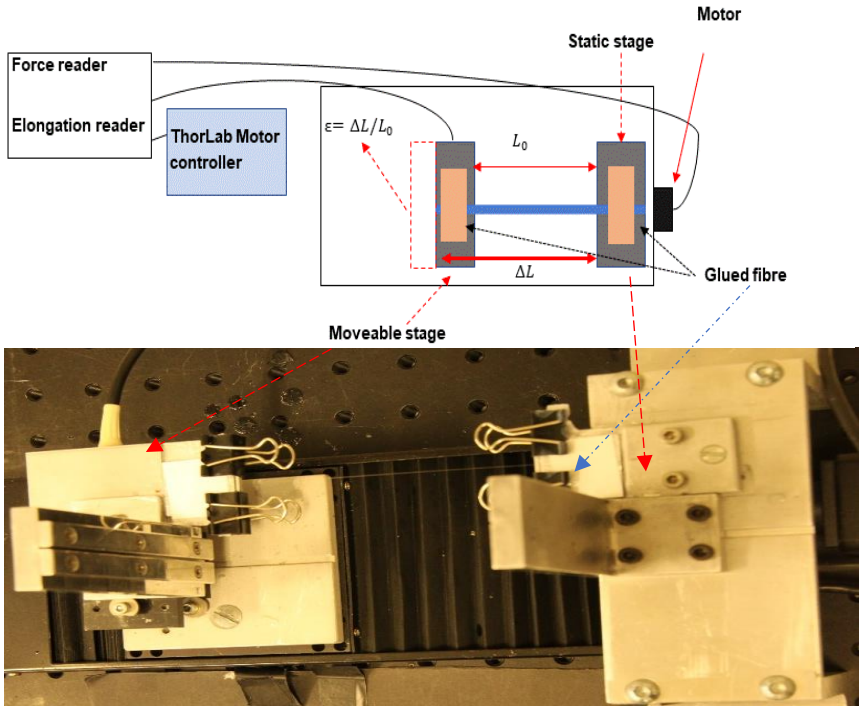

Figure 6. Schematic figure of the experimental setup of the tensile test measurements.

One of the stages of the gauge length machine moves with speed of 0.03 mm/s, which is considered sufficient to spread the stress equally along the fibre surface. Other speeds, tested between 0.01mm/s to 0.3mm/s, are not found to significantlly affect force at failure (see Figure 7). The moving stage cell is connected to a computer to record stage displacement and the force that the stage applies onto the fibre until fibre failure, while the other stage is static, as shown in Figure 6. The anchored fibre on two stages is pulled and the relative elongation ε is output as a function

of applied force until the fibre fails. The relative elongation is measured by recording the change in the length of the fibre known as absolute elongation, ΔL, given in Equation 3.2.

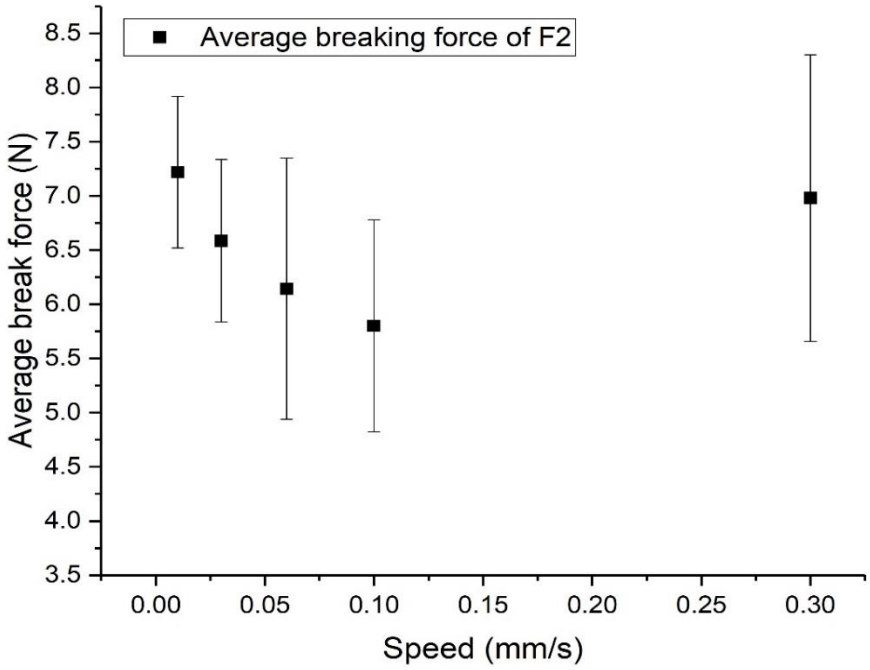

Figure 7. Average breaking force at different speed of F2c solid glass fibre.

The fibre can be bent (curved) due to its own weight or when covered with paper which is used to support fibre gluing. Due to this bend, the applied force will read zero on the computer until a non-zero force is applied to the fibre (when fibre is taut) as shown in Figure 8. The part of the recorded force vs elongation graph for which the force is zero (while the fibre is still slack) is eliminated by shifting the zero point of the graph in post-processing. Further, when the fibre fails, the force abruptly drops to zero. The point of the curve at which this occurs represents the force at which the fibre fails. Another important point which need to mention here is that at the early stage of this project it has been found that fibre failure were sensitive to curing time and method of securing fibre ends to the stage. A carful arrangement of the apparatus as well as curing time for 15 min were found to fully address the issue of the fibre failure at the edge of the plate or inside the glue. Additionally, the number of fibre that failed at the edge of the stage or in the glue were not included in the results.

4.3 – Processing of mechanical and statistical collected data

The experimental data collected allows the plotting of force versus elongation for each fibre sample before the fibre breaks. Figure 9a shows a representative result of the elongation of the solid SMF28(F300) fibre under applied force. The point where the curve ends represents the fibre failure. The average breaking force of solid SMF28(F300) fibre stripped mechanically was

measured to be 8.0±1.5 N, which is consistent with the reported result of 7.47 N [1]. The error of the average breaking force is calculated using the standard error of the mean. This technique is used for all the other fibres in this experimental work. Figure 9b shows force at failure (force at which fibre breaks) versus maximum relative elongation (i.e. elongation at failure) for each individual fibre sample. The fitted slope value is used to determine the fibre's Young's modulus. The error on the slope represents the error in the Young's modulus. The result for SMF28(F300) fibre gives a Young's modulus of 68.6 ± 1.7 GPa, which is consistent with the reported value of the solid SMF28(F300) fibre's Young's modulus of 69.22 ± 0.42GPa [1], 71.8 GPa [54].

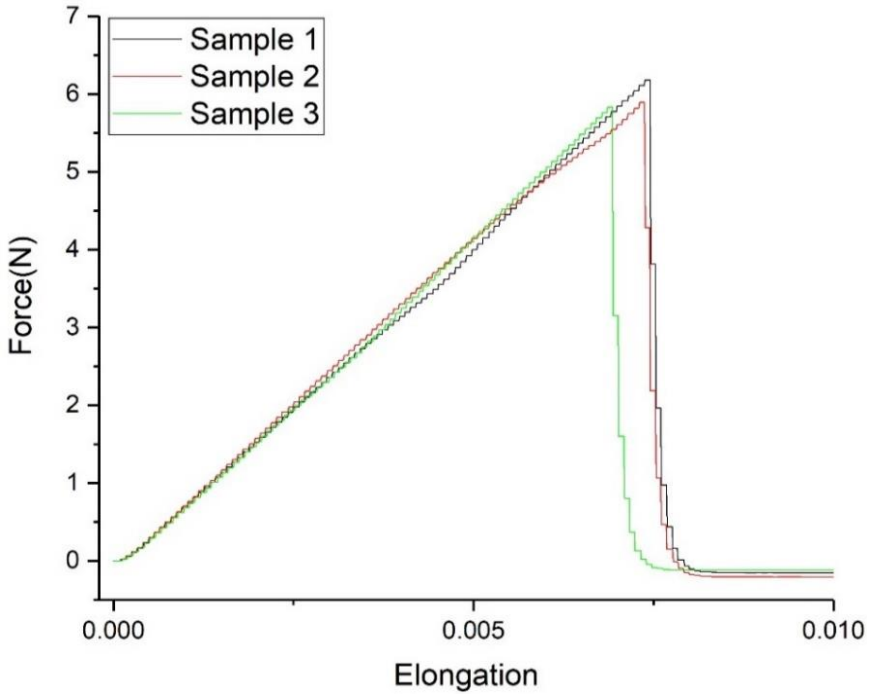

Figure 8. Raw data of fibre elongation under tensile force of SMF28(F300).

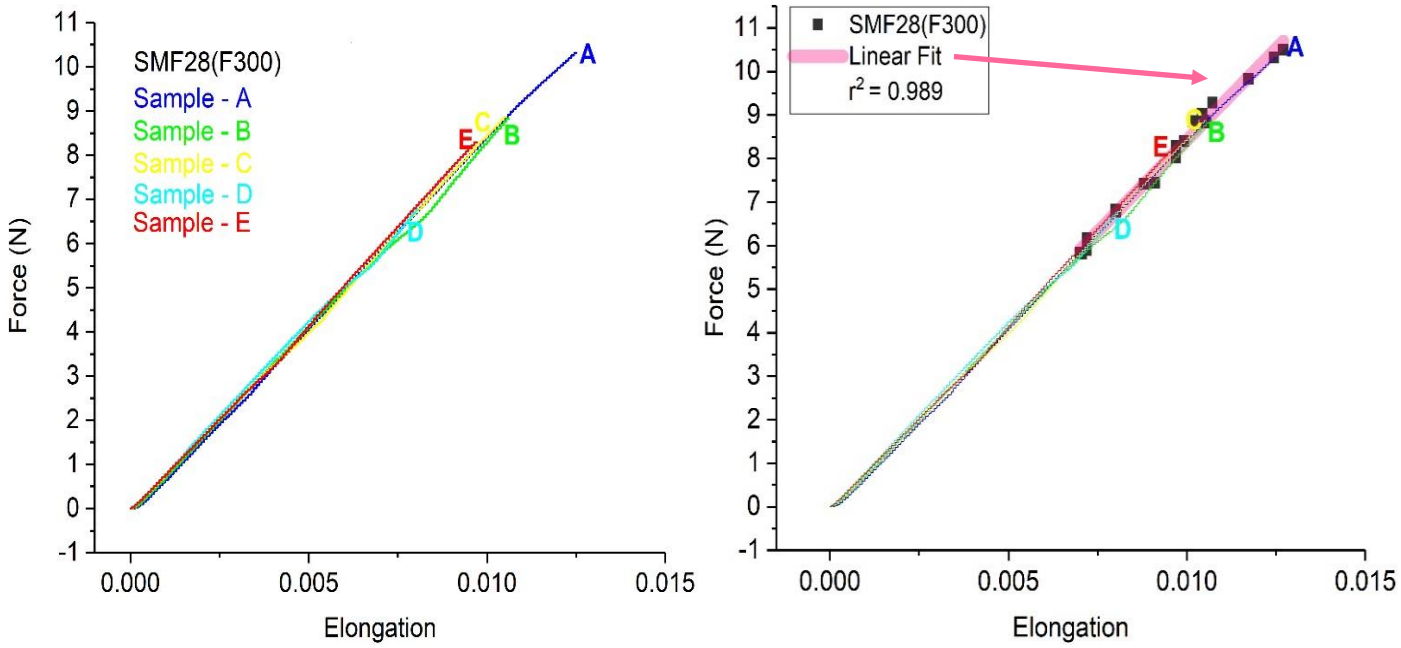

a *b*

Figure 9. Force versus elongation data of standard optical fibre SMF28(F300) with coating stripped mechanically for a) representative samples b) all data, with the force at failure highlighted by black squares, and linear fit for force at failure data.

As can be seen from Figure 9b, the slope of force at failure vs elongation at failure follows the same slope as for the curve of force vs elongation in Figure 9a for each sample.

The values of force at failure are used to calculate stress at failure using Equation 3.4. The stress at failure of the fibres are ranked in order, from smallest to greatest, in order to find the median ranking of each fibre failure of solid SMF28(F300) data as shown in Table 2. The natural logarithm (Ln) of stress at failure of each fibre as well as the double Ln of median fibre failure are found following Equation 3.8 and shown in Table 2 in the last two columns. Values in these columns are used to generate two parameter (unimodal) Weibull distributions as shown in Figure 10. The slope value and intercept (when converting Equation 3.8 into linear form) are used to calculate the characteristic strength of the fibre as follows [53]:

$$\sigma_0 = e^{-\frac{b}{m}}, \qquad 4.1$$

where $b = m\,ln\,\sigma - ln\left(ln\left(\frac{1}{1-P}\right)\right)$ and m is the Weibull slope. The error in the fitted slope in Figure 10 and the intercept are used to define the error of the σ_0 derived from the following error propagation formula for a function $Q(a, b, \dots)$:

$$\frac{\partial Q}{|Q|} = \sqrt{\left(\frac{\partial a}{a}\right)^2 + \left(\frac{\partial b}{b}\right)^2 + \cdots}, \qquad 4.2.$$

Table 2. Statistical analysis of the collected data to generate Weibull distribution of SMF28(F300) fibre (see full Table in Appendix A).

N –total fibre tested	Ascending order of fibre failure ***i***	Fibre Stress to failure σ (GPa)	Median rank $P = \frac{i - 0.3}{N + 0.4}$	**Ln (σ (GPa))**	**Ln (Ln(1/1-F))**
Shown only 5 of 20	1	0.47362	0.03431	-0.74735	-3.3548
	2	0.4755	0.08333	-0.74339	-2.44172
	3	0.48073	0.13235	-0.73244	-1.95214
	4	0.50395	0.18137	-0.68527	-1.60881
	5	0.55213	0.23039	-0.59396	-1.33989

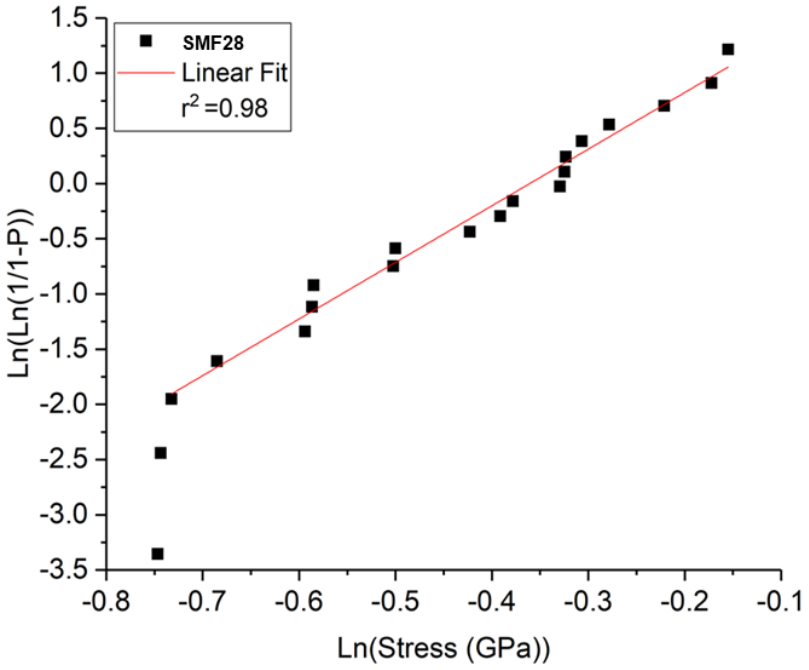

Figure 10. Weibull distribution plot of the measured failure population data of SMF28(F300) fibre stripped mechanically represented by black squares and the line is regression line using linearized two-parameter (unimodal) Weibull distribution (note: first two points considered as outliers, therefore were excluded).

In Figure 10, the probability failure of the solid SMF28(F300) fibre treated with a unimodal Weibull distribution is shown. The linear regression fit does not include the first two samples (10% of the samples), because of their abnormally low stress at failure. This indicates that first two samples were mechanically damaged while handling or gluing on the stage and is not representative of

the fibre on the drum, and that those two points are more an experimental error rather than a real fibre failure due to extrinsic defects.

Depending on the distribution of the failure population in the Weibull plot, different fitting techniques can be used to obtain Weibull parameters in order to characterise the mechanical strength of the optical fibre. For instance, if one straight line cannot be well fitted to plotted data points of failure distribution using two-parameter Weibull distribution function or three-parameter Weibull distribution function, both of which are known as unimodal Weibull distributions (see Equations 3.8 and 3.10), then two straight lines for two different sub-sets of the measured failure population data might be necessary to achieve a good fit to the measured data in order to extract the physical meaning of the sub-set measured failure. The technique where two lines are fitted to two different sub-sets of the measured failure population is known as bimodal Weibull distribution. If the data set of measured failure population can only be well fitted with two lines, this indicates the presence of more than one type of defect, which causes that failure population to be distributed in (two) different modes [51, 55, 56]. This Weibull distribution is used widely to analyse experimental results and contains two distinct slopes. In the bimodal Weibull distribution, failure population is associated to two regions; zones 1 and 2. In zone 1, the distribution has a higher m value, where failure distribution has little variation, and in zone 2, has a lower slope value, where failure distribution has high variation [50, 51, 57].

To obtain Weibull parameters of each distinct population in a bimodal Weibull distribution, failure population is split in two sub-populations as shown in Figure 11 for F2b solid glass fibre which is described in section 4.1 and listed in Table 1. The procedure for this splitting is as follows:

1. The probability of failure is obtained using the median rank approximation from Equation 3.9.
2. The values obtained from the median rank approximation are plotted against the ordered data (stress at failure) in a Weibull distribution plot.
3. The point at which the distinct sub-populations are split is determined by the point at which the r^2 values of the corresponding regression lines is maximised.
4. The median rank approximation for each sub-population is then determined separately using Equation 3.9 – a repeat of step 1 for each sub-population.
5. Data from the separated sub-populations are plotted in another Weibull distribution plot (see Figure 11b) – a repeat of step 2 for each sub-population.
6. Weibull parameters are obtained for each sub-population.

A bimodal Weibull distribution is used to distinguish between two types of failure, the low stress at failure (sub-population 1), and high stress at failure (sub-population 2) (Figure 11 b).

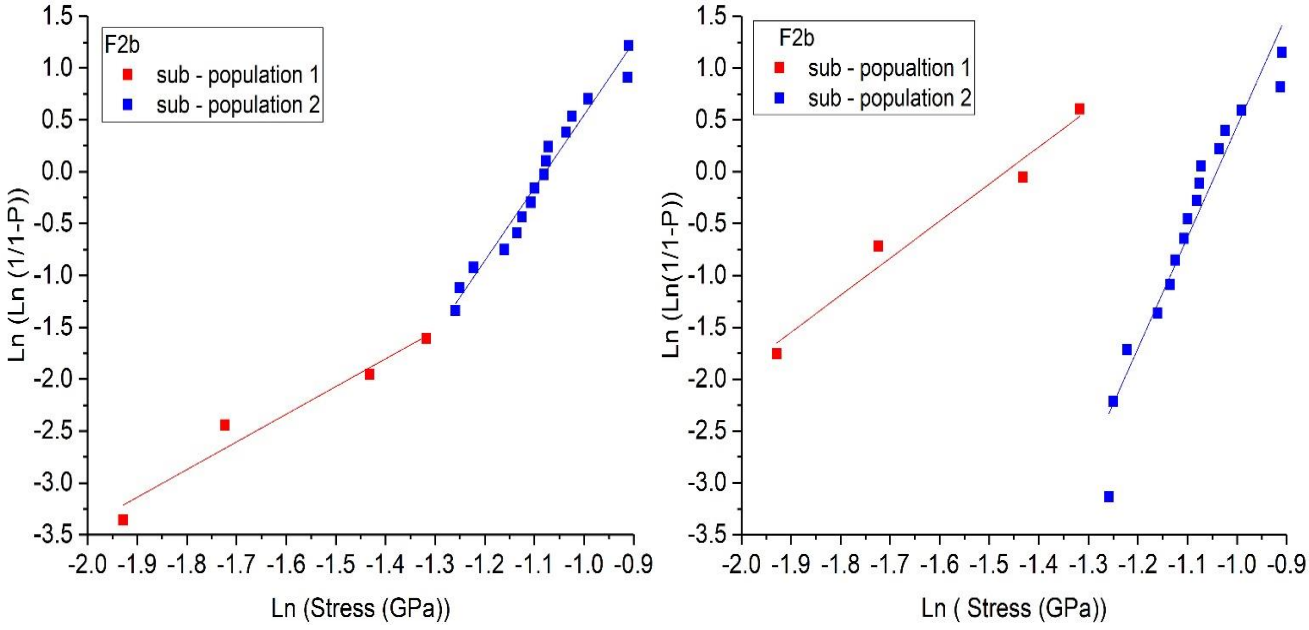

a b

Figure 11. An example of data distributed in more than one mode, in a) determination of sub-population fitted with linear regression for each sub-population and b) bimodal Weibull distribution plot of data set and linear regression lines of the representative sub-populations.

4.4 – The Young's modulus and Weibull model outcome of solid fibres made from different glass materials

Based on the tensile measurement and characterisation methods shown in section 4.2, the experimental work was conducted on solid fibres made of various glass material, shown in Table 1. The experimental results of mechanical properties for these glass optical fibres are shown in Table 3.

Data in Table 3 is plotted in Figure 12, which shows significant difference between the Young's modulus of all of the solid glass fibres tested here. The Young's modulus value of the SMF28(F300) fibre overlaps with reported Young's modulus values of the solid LWQ glass fibre. F2a fibre shows a lower Young's modulus value compared to LWQ, Ge and Duran solid fibres. Additionally, it is important to point out that the values of the Young's modulus of solid Duran, Ge, F2, ZBLAN and Te glass fibres differ from the reported values of bulk glass shown in last column of Table 3. It is worth noting here that the Ge and Te solid glass fibres were a different composition to the exact glass material referred in third column of Table 3. However, in some cases, reduction of the fibre size leads to increased ductility (reduced Young modulus) [58, 59]. This behaviour was observed in some of the glass fibres tested here.

The statistical analysis of the measured failure of silica and hard glass solid fibre shows a unimodal Weibull distribution, while soft glasses Ge, Te, and ZBLAN solid fibres show bimodal

Weibull distribution (see Figure 13). F2 solid fibre is at the borderline as it can be reasonably well fitted with a unimodal distribution or bimodal Weibull distribution. As can be seen from Table 4 and 5 the slope value and characteristic strength of both Weibull distributions are very similar, which allows comparing soft glass F2 with silica and hard glasses (Figure 13).

Table 3. Results and reported values of Young's for various glass optical fibres.

Fibre glass	Young's modulus (GPa)	Reported value of Young's modulus (GPa)
LWQ	70.6 ± 1.5	69 – 73 *[1, 54]*
SMF28(F300)	68.6 ± 1.7	69 – 73 *[1, 54]*
Duran	53.5 ± 1.2	64 [60]
Ge	49.7 ± 1.3	63.6 [61]
F2a	47.6 ± 0.4	57 [60]
ZBLAN	41.7 ± 1.1	53 [62]
Te	37.0 ± 2.1	39 – 62 [63]

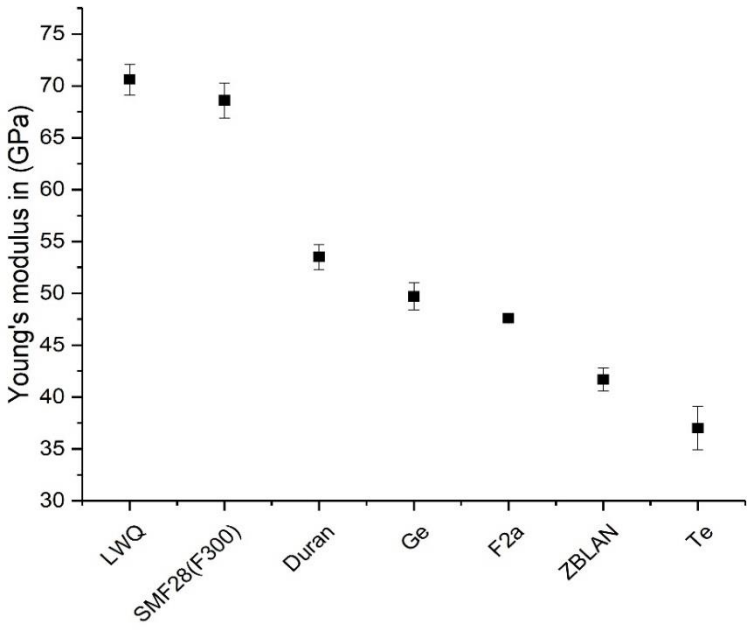

Figure 12. *Young's modulus values of the solid fibre made of different glass material listed as in Table 3.*

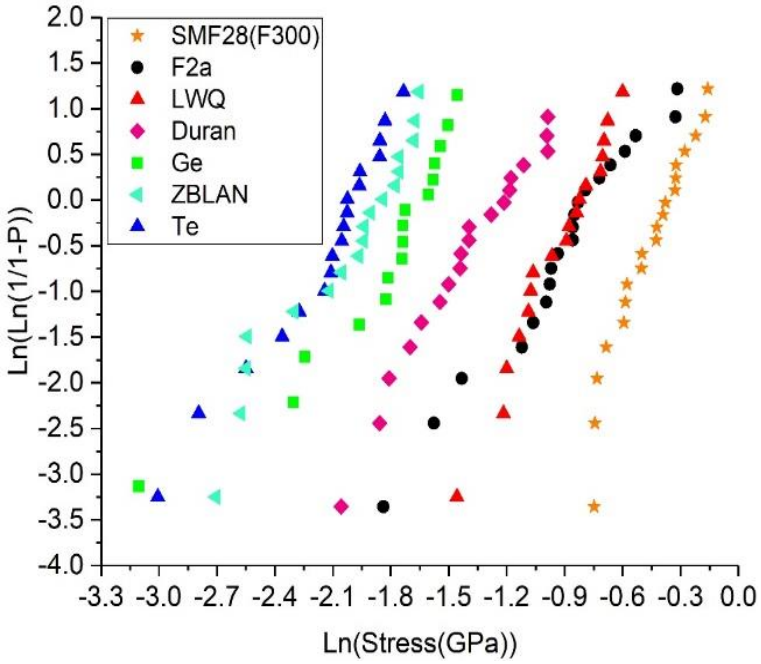

Figure 13. Weibull plot of data of solid fibre made of silica glass (SMF28(F300), LWQ), Duran glass, and soft glasses such as F2, Ge, Te, ZBLAN.

Figure 13 indicates that the lower stress at failure value of solid F2 glass fibre compared to SMF28(F300) follows the same trend as for Young's modulus, shown in Figure 12. However, results shown in Figure 12 and 13 show that the stress at failure of solid F2 glass fibre relative to solid LWQ and Duran glass fibre did not follow the trend of the Young's modulus values. Lower stress at failure of solid Duran glass fibre compared to solid SMF28(F300) and solid LWQ fibre followed the trend of the Young's modulus values in Figure 12. Table 4 summarises the results of Weibull parameters such as characteristic strength and Weibull slope of solid SMF28(F300), F2a, LWQ and Duran fibre failure distribution. Results indicate that the reliability of the solid F2a glass fibre is lower than reliability of SMF28(F300), LWQ and Duran solid glass fibre as can be seen from the Weibull slope values.

Additionally, higher stress at failure of solid F2 glass fibre compared to other soft glass fibre such as Te and ZBLAN followed the trend of the Young's modulus value, however higher stress at failure of solid F2 glass fibre compare to solid Ge glass fibre did not follow the trend of the Young's modulus values (see Figure 12 and 13).

Table 4. Characteristic strength and Weibull slope of fibres obtained using unimodal (two – parameter) Weibull distribution.

Fibre glass	Characteristic strength σ_0 (GPa)	Weibull slope m
SMF28(F300)	0.69 ± 0.04	5.1 ± 0.2
F2a	0.48 ± 0.03	3.0 ± 0.1
LWQ	0.44 ± 0.02	5.3 ± 0.2
Duran	0.29 ± 0.01	3.7± 0.1

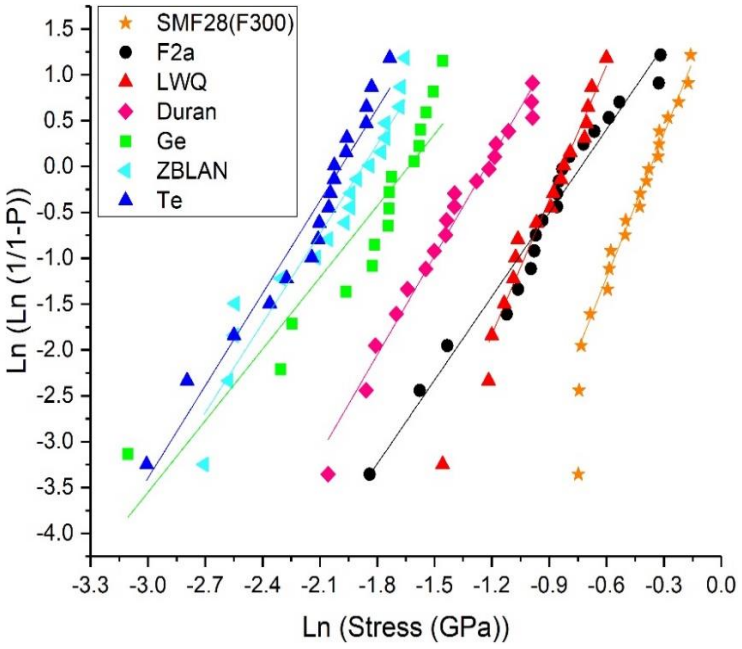

Figure 14. Lines of fitting the whole data set (except outliers) of Weibull distribution plot of measured failure population data of solid fibre made of F300 (SMF28(F300)), LWQ and Duran and soft glasses (F2a, Ge, Te, ZBLAN).

Figure 14 shows the linear regression fit of unimodal Weibull distribution model used for analyses of measured distribution of failure population of the solid fibres made of silica, Duran and soft glass (F2, Ge, Te, ZBLAN). The result in this figure indicates that the failure populations of solid soft glass fibre such as Ge, Te and ZBLAN are characterised by more than one defect type, and as a result the bimodal Weibull distribution is employed (see Figure 15). Table 5

summarises the results of the characteristic strength and the bimodal Weibull distribution slopes for both sub-populations of the soft glass solid fibres tested in this work.

Table 5. Characteristic strength of the glass optical fibre for both sub-population and their reliability (Weibull slope value).

Fibre glass	Number of points for sub-population	Characteristic strength of sub-population 1 σ_o (GPa)	Weibull slope of sub-population 1 (m_1)	Number of points for sub-population	Characteristic strength of sub-population 2 σ_o (GPa)	Weibull slope of sub-population 2 (m_2)
F2a	4	0.26 ± 0.06	3.3 ± 0.4	16	0.5 ± 0.1	4.6 ± 0.6
Ge	10	0.17 ± 0.01	2.3 ± 0.4	6	0.23 ± 0.01	18.5 ± 3.0
ZBLAN	6	0.1 ± 0.01	4.5 ± 1.0	12	0.17 ± 0.002	8.4 ± 0.6
Te	6	0.09 ± 0.001	3.2 ± 0.2	12	0.14 ± 0.01	8.8 ± 1.2

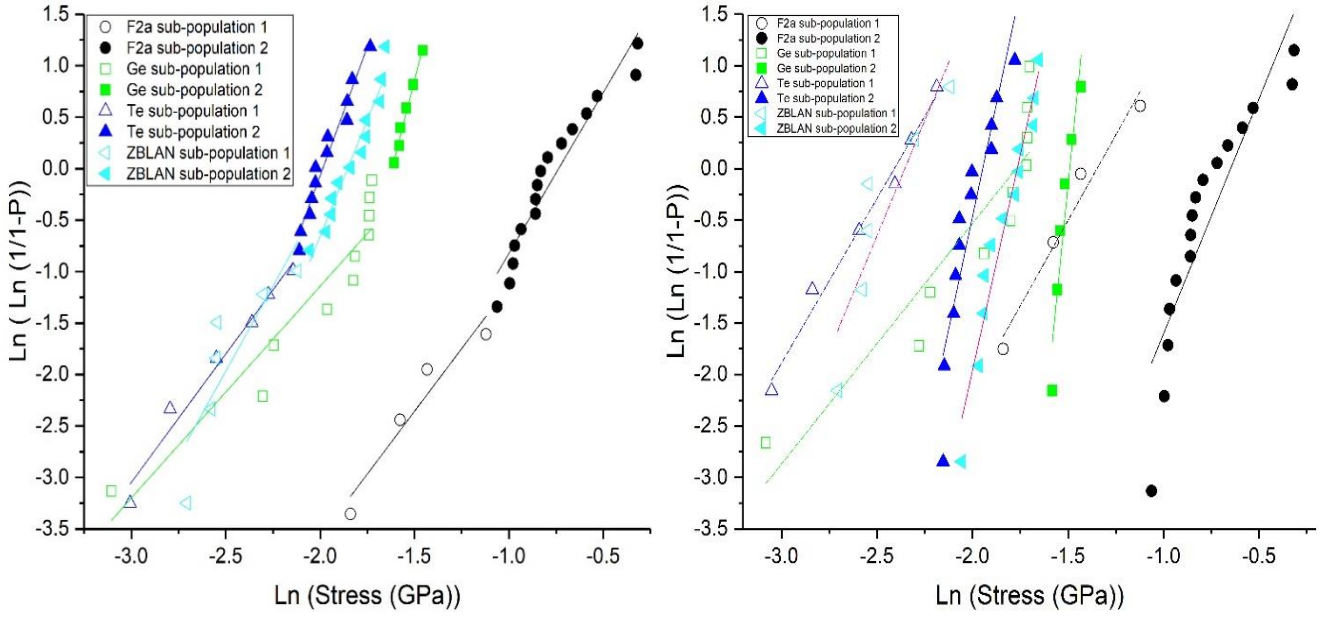

a *b*

Figure 15. Weibull plot of data of solid fibre made of soft glass a) determination of sub-population data fitted with linear regression fit for each sub-population b) bimodal Weibull distribution plot of data set and linear regression lines of the representative sub-populations.

4.4.1 – Analysis and discussion

The mechanical properties of glass optical fibres such as the Young's modulus are obtained by using uniaxial tensile test method, and shows that glass materials can have a high Young's

modulus E but can be characterised with low characteristic strength σ_0, as is the case with LWQ glass solid fibre (high E, low σ_0) compared to F2 glass solid fibre (low E, relatively high σ_0). This strongly indicates that defects along the fibre determine the characteristic strength.

Weibull distribution of failure population data in Figure 13 and 15 indicates that the solid fibres made of soft glasses such as Ge, ZBLAN and Te are distributed in more than one mode. This indicates that the failure at soft glass is due to more than one types of defects. Therefore, bimodal Weibull distribution is employed to determine their characteristic strength.

The SMF28(F300) optical fibre, LWQ and Duran solid fibre shows that the distribution of the failure population is unimodal and narrowly distributed (higher Weibull slope *m* value) which indicates that failure is generated by one type of defects. Results in Figure 12 and 13 indicate that the characteristic strength of the solid fibres made of different glass material follows the Young's modulus values. By decreasing the Young's modulus value, the characteristic strength of solid glass fibres decreases. However, results shown above indicates that solid F2 glass fibre is an exception and does not follow the relationship between Young's modulus and characteristic strength compared with LWQ, Duran and Ge solid fibres, which would benefit from future studies.

4.5 – Comparison between aged (stored) and non – aged lead silicate glass solid fibre

Using the mechanical characterisation method of force vs elongation shown above in Figure 9 and 10 allows us to obtain Young's modulus values of F2 solid glass fibres fabricated at different times. See the data tabulated in Table 6. It should be noted with this data that small variation in fabrication condition and parameters it may also influence the Young's modulus values between fibres.

The collected data from the uniaxial tensile test allows the presentation of the Weibull distribution of the failure population of the stored, uncoated F2 solid glass fibres fabricated at different dates (see Figure 16). The fabrication dates shown in Table 6, vary from 2011 for F2d, 2013 for F2c, 2017 for F2b, and F2a fabricated in 2018. Figure 16a shows the failure populations of stored solid F2 fibres plotted using two parameter Weibull distribution (unimodal Weibull distribution) and Figure 16b shows linear regression fit of data plotted with unimodal Weibull distribution. The results indicate that the distribution of the failure population of the stored F2 solid glass fibre has more than one mode. Therefore, bimodal Weibull distribution is employed to analyses the data, as can be seen in Figures 17. The distribution of the failure population of the F2 solid glass fibre is split into two sub-populations (see Figure 17) using the method described in section 4.3. Table 7 summarises the results of the characteristic strength and the bimodal Weibull distribution slopes for both sub-populations of the F2 solid glass fibres tested in this work.

Even though the difference in fabrication dates is large, the characteristic strength of the fibre is the same within error, and failure population is distributed in same region between Duran and SMF28(F300) solid fibre as shown in Figure 16a. However, the distribution of the failure population is different for different fabrication dates, as shown by the Weibull slope value in Table 7.

Table 6. Young's modulus value of aged (stored) F2 solid fibre.

Fibre glass	Young's modulus (GPa)	Fabrication date	Aging in (months)
F2d	46.8 ± 0.8	2011	84
F2c	48.3 ± 0.6	2013	60
F2b	49.2 ± 1.2	2017	12
F2a	47.6 ± 0.4	2018	One week

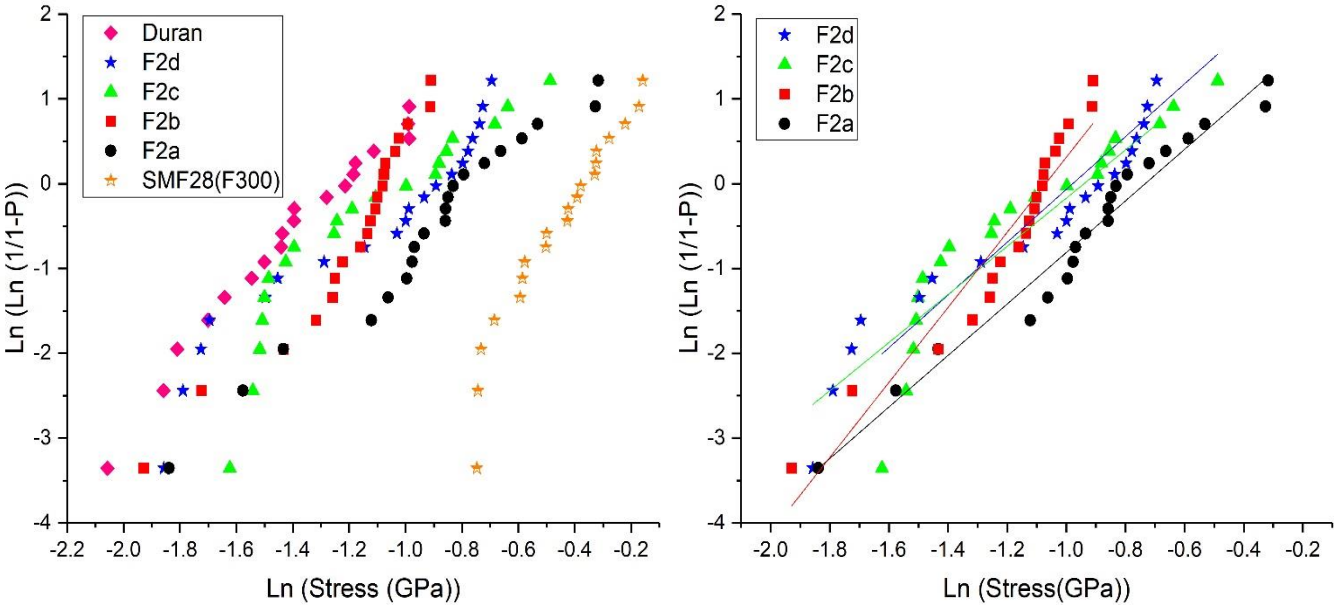

a *b*

Figure 16. Weibull plot of data of a) F2, Duran and SMF28(F300) solid glass fibre b) linear regression fit of F2 data plotted as unimodal Weibull distribution.

Table 7. Characteristic strength of the stored F2 solid glass fibre for both sub-population and their reliability (Weibull slope value).

Fibre glass	Aging in (months)	Number of points for sub-population	Characteristic strength of sub-population 1 σ_o (GPa)	Weibull slope of sub-population 1 (m_1)	Number of points for sub-population	Characteristic strength of sub-population 2 σ_o (GPa)	Weibull slope of sub-population 2 (m_2)
F2d	84	11	0.29 ± 0.06	3.2 ± 0.4	9	0.47 ± 0.02	13.9 ± 0.6
F2c	60	6	0.22 ± 0.08	20.2 ± 3.4	14	0.43 ± 0.05	3.9 ± 0.3
F2b	12	4	0.23 ± 0.06	3.8 ± 0.5	16	0.35 ± 0.01	13.1 ± 1.8
F2a	One week	4	0.26 ± 0.06	3.3 ± 0.4	16	0.5 ± 0.1	4.6 ± 0.6

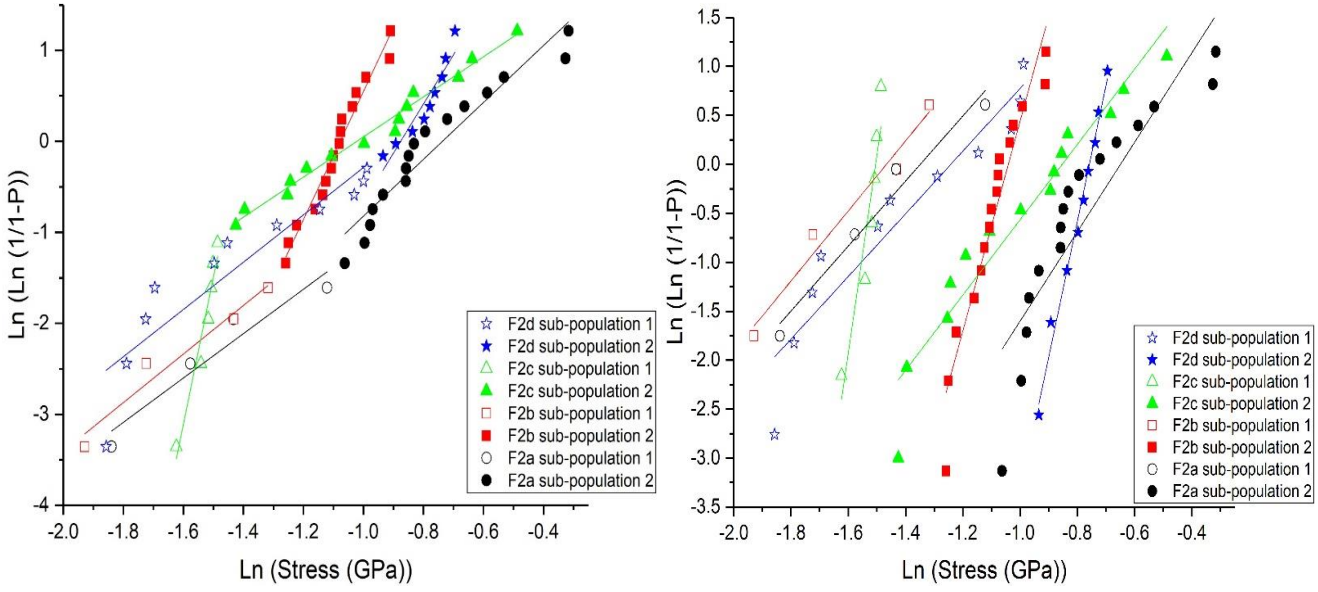

Figure 17. Weibull plot of data of all F2 solid glass fibres, a) Determination of sub-population data fitted with linear regression fit for each sub-population and b) bimodal Weibull distribution pot of data set and linear regression lines of the representative sub-populations.

4.5.1 – Analysis and discussion

The results shown above indicate that the aging effect in the F2 solid glass fibre does not significantly affect mechanical properties or statistical failure distributions. Furthermore, collected

data indicates a relationship between the Young's modulus of the fibre with the characteristic strength, even though the Young's modulus is a glass property, whereas characteristic strength depends on the defects on the fibre. Results shown in Table 7 indicates that the aging effect of solid F2 glass fibres is not significant in terms of the strength in general, since all F2 fibres did fail at a region between Duran and SMF28(F300) solid fibre (see figure 16 a). As can be seen in this case, the failure population of solid F2 glass fibres is distributed in a broad range of stress at failure, which indicates the presence of more than one defects types on the solid F2 glass fibre due to the fabrication process, handling and moisture in the storage room.

4.6 – The effect of capillary hole size (inflation ratio) and of different inner structural geometry on the strength glass optical fibre.

This section discusses the impact of the holes on strength of the fibre, with investigating two different fibre types with holes such as capillary fibre and SCF. The results of tested capillary fibres with different holes sizes (inflation ratio) and SCF made of F300 glass materials are compared with SMF28(F300) fibre, whereas SCF made of LWQ glass material is compared with SCF made of F300 glass and LWQ solid glass fibre.

4.6.1 – Inflation ratio and suspending core fibre (SCF)

The capillary fibre (see Figure 18a) was made from a preform tube where gas pressure was used to inflate the inner hole in order to make capillary fibres with differently sized inner holes, while keeping the outer diameter fixed. The effective cross sectional area is the solid fraction of the capillary fibre. The fibre material and diameter of the inner hole of the capillary fibres is shown in Table 1. SCFs are made using the drilling technique to fabricate the SCF preform (see Figure 18b). The red circle drawn in the cross sectional area of the SCF (Figure 18b) was used as a means to allocate an ID value to a SCF to allow investigation of the impact of ID/OD ratio on the mechanical strength of SCF. To do so, it is necessary to relate the multi hole geometry structure to a single capillary geometry, therefore hole diameter (red circle) is defined as the diameter of a circle which has the same circumference as that of the sum of the inner holes [64, 65].

The tensile measurement and mechanical characterisation were conducted on the capillary glass optical fibres made of F300 glass material, and SCFs fibre made of LWQ and F300 glass material, respectively. Table 8 summarises the results of the Young's modulus values of solid SMF28(F300) fibre, all capillary fibres and SCFs. Data from Table 8 are plotted in Figure 19, which indicates that the Young's modulus value of all capillary fibres and SCFs overlap with Young's modulus value of SMF28(F300) fibre within errors.

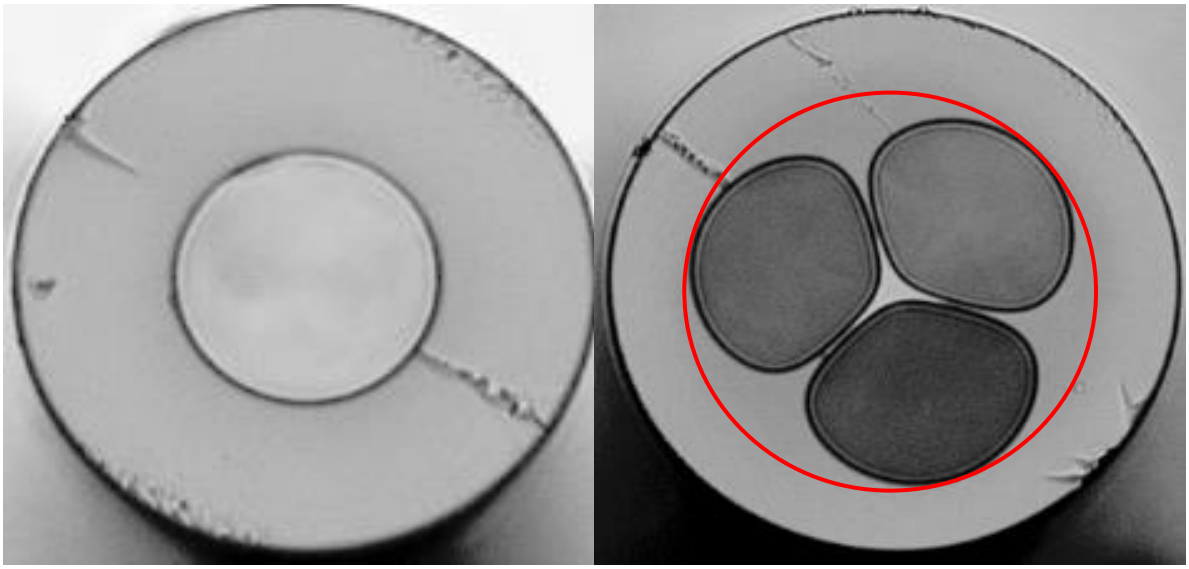

a *b*

Figure 18. Cross sectional image of the a) capillary fibre F300 – C3 made of F300 glass material, b) SCF's made of F300 glass material.

Table 8. The Young's modulus of the F300s (capillary), LWQ – SCF, F300 – SCF, LWQ and SMF28(F300) solid fibre.

Fibre glass	Young's modulus (GPa)	Ratio ID/OD
SMF28(F300)	68.6 ± 1.7	0
F300 – C1	69.0 ± 1.0	0.029 ± 0.001
F300 – C2	69.5 ± 1.2	0.32 ± 0.02
F300 – C3	68.2 ± 1.2	0.45 ± 0.02
F300 – C4	70.0 ± 1.1	0.53 ± 0.03
F300 – C5	71.7± 0.8	0.60 ± 0.03
F300 – SCF	68.4 ± 2.0	0.45 ± 0.02
LWQ – SCF	67.9 ± 1.2	0.45 ± 0.02
LWQ	70.6 ± 1.5	0

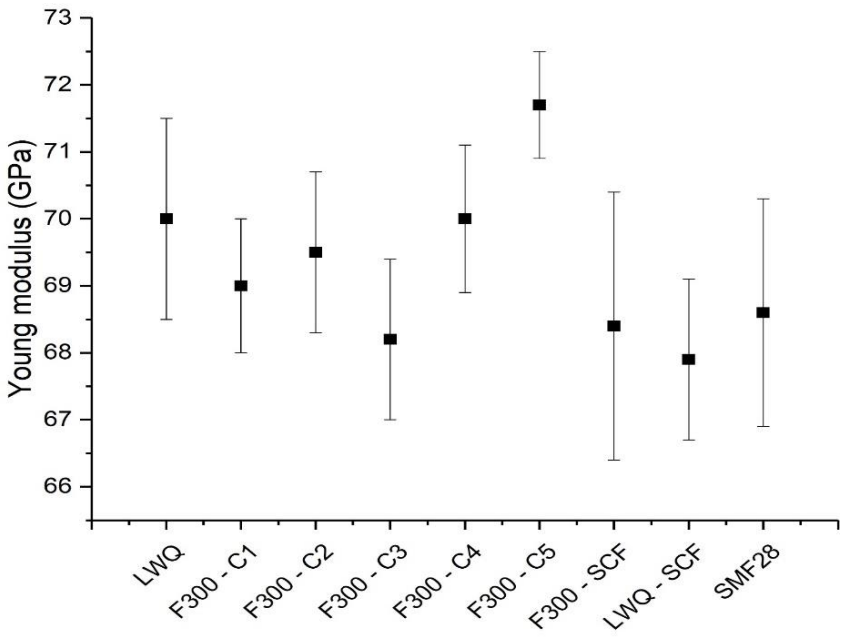

Figure 19. Young's modulus of the silica fibres listed as per Table 8.

The statistical analyses of the data collected from uniaxial tensile test of the capillary and SCFs glass fibre were treated with a unimodal Weibull distribution (see Figure 20). The Weibull slope of the distribution of the failure population of F300 – C1 and F300 – C2 (See Table 9 and Figure 20b) is the same, even though the hole size is slightly different. By increasing hole diameter (inflation ratio) the distribution of failure population increases (become broaden), as can be seen in Figures 20. This results in a lower Weibull slope value (Table 9) compared with solid SMF28(F300) and SCFs. Also, the results indicate that the capillary fibres have lower characteristic strength values than solid SMF28(F300), but have the same characteristic strength, within error, as the F300 – SCF. This similarity in strength of capillary fibres and F300 – SCF is attributed to the similarity in their ID/OD ratio (valid for F300 – C3 vs F300 – SCF, see Table 8). The results summarised in Table 9 indicate that the changes to the hole size in the fibre do not significantly effect the characteristic strength of the capillary fibres. The results shown in Table 9 and Figure 20b indicates that both SCFs have lower characteristic strength than SMF28(F300), but have higher Weibull slope value than solid SMF28(F300).

Table 9. Characteristic strength and Weibull slope for fibres treated with unimodal Weibull distribution.

Fibre	*Characteristic strength* σ_o *(GPa)*	*Weibull Slope m*
SMF28(F300)	0.69 ± 0.04	5.1 ± 0.2
F300 – C1	0.54 ± 0.02	4.5 ± 0.1
F300 – C2	0.56 ± 0.02	4.5 ± 0.1
F300 – C3	0.53 ± 0.02	2.9 ± 0.1
F300 – SCF	0.51 ± 0.03	6.4 ± 0.2
LWQ	0.44 ± 0.02	5.3 ± 0.2
LWQ – SCF	0.43 ± 0.02	7.3 ± 0.3

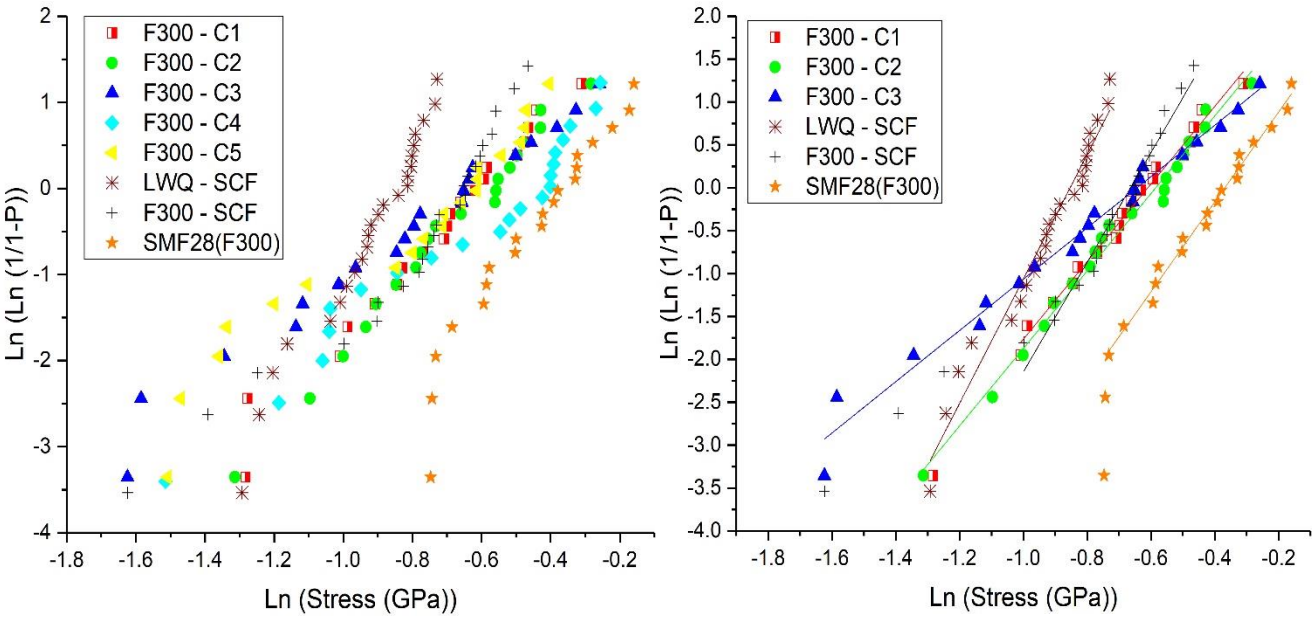

a *b*

Figure 20 Weibull plot of data of a) F300s capillary (fibres with one hole), SCFs and SMF(F300) fibres, b) linear regression fit of F300 – C1, C2, C3, LWQ – SCF, F300 – SCF, SMF28(F300) data as unimodal Weibull distribution.

The distribution of the failure population of capillary fibres shown in Figure 20a indicates that capillary fibres such as F300 – C4 and F300 – C5 have more than one mode. Therefore, the bimodal Weibull distribution is employed to analyse the data (see Figure 21). These two fibres

have the largest inflation ratio from all capillary fibre that is 0.53 ± 0.03 for F300 – C4 and 0.60 ± 0.03 for F300 – C5.

Table 10 summarises the results of the Weibull parameters of both sub-population of the F300 – C4 and F300 – C5 obtained using the bimodal Weibull distribution technique. The results shown below indicates that by increasing the inflation ration, different defects in the fibre are introduced, resulting in different modes of distribution of the failure population.

Table 10. Statistical results of the F300 – C4 and F300 – C5.

Fibre	Number of points for sub-population	Characteristic strength σ_o (GPa) of sub-population 1	Weibull Slope m_1	Number of points for sub-population	Characteristic strength σ_o (GPa) of sub-population 2	Weibull Slope m_2
F300 – C4	11	0.46 ± 0.04	3.7 ± 0.2	10	0.7 ± 0.1	15.1 ± 2.0
F300 – C5	6	0.29 ± 0.02	6.5 ± 1.0	14	0.57 ± 0.01	8.3 ± 0.5

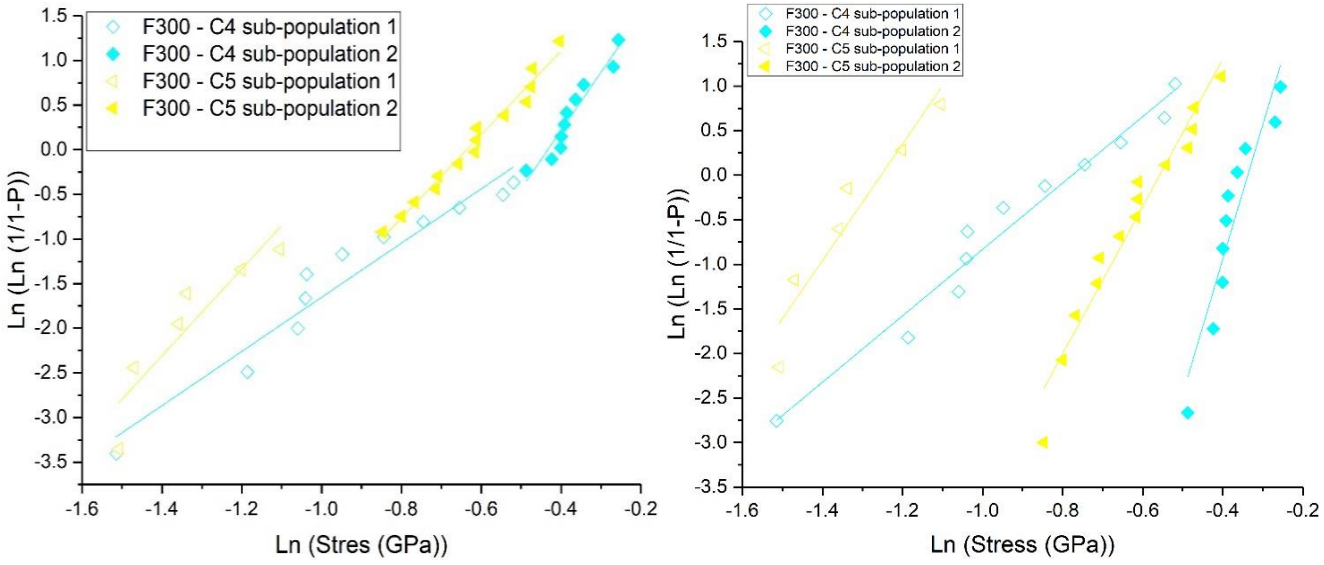

a *b*

Figure 21. Weibull plot of data set of F300 – C4 and C5, a) determination of sub-population data with linear regression fit for each sub-population and b) bimodal Weibull distribution plot of data set and linear regression lines of the representative sub-populations.

A comparison of distribution of failure population of C2 and C3 fibre with second sub-population of C5 shows the Weibull slope is different; however, the characteristic strength is the same within error (see Table 9 and 10). This indicates that the ratio ID/OD did not change fibre characteristic strength, but it did change failure distribution.

4.6.2 – Analysis and discussion

The previous section covered the tensile test results of capillary fibres and SCF. The results show, in general, that the distribution of the failure population of the capillary fibre (F300 – C1, F300 – C2 and F300 – C3) is relatively insensitive to the ID/OD at low inflation levels shown in Figure 20b. Indeed, the capillary fibre strength does not vary significantly with respect to low inflation ratio (small changes in hole size), as can be seen in Tables 9. Though capillary fibres have lower characteristic strength compared to solid SMF28(F300) fibre with the same outer diameter 125 µm, in general, the higher the inflation ratio, the less reliable the fibre (see Weibull slope in Table 0). Based on Table 9, it can be concluded that the characteristic strength of the capillary fibres is similar for all hole sizes, which is valid for F300 – C1, F300 – C2 and F300 – C3. This suggests that neither the presence nor the size of holes significantly effects the characteristic strength of the fibre along its tensile axis, which is an interesting result. However, the Weibull distribution of the capillary fibre F300 – C4 and F300 – C5 shows more than one mode of distribution of the failure population. Note these fibres have larger inflation ration (see Table 8). Furthermore, the results of the SCF tests also suggest that the number of holes does not significantly affect the characteristic strength of the fibre, although the reliability (distribution of failure population) of the fibre is indeed affected by showing higher slope value compared with solid SMF28(F300) fibre as shown in Table 9. The LWQ – SCF shows the same characteristic strength, but higher reliability (Weibull slope) compared to the LWQ solid fibre (see Table 9). Additionally, the LWQ – SCF shows lower characteristic strength but higher reliability (Weibull slope) compared to F300 – SCF (see Table 9), where both fibres have same ID/OD ratio.

Chapter 5 – Optical Characterisation of Loss and Raman Signal of Glass Optical Fibres

5.1 – Introduction to Optical Characterisation

In recent years, there has been an increased interest in research related to the application of biomedical sensing using fibre-optic probes [66]. The main reason behind this interest is that optical fibres can provide access to otherwise inaccessible parts of an organism [6]. The main challenge when using optical fibres is the ability to obtain good signal to noise ratios. Therefore, sensing applications require the maximum amount of signal to be collected by the fibre, while minimising its optical losses [25].

In this chapter, work is focused on measuring transmission loss of solid Duran, F2 fibre, and HCFs made of F2 glass. To make an extruded Duran HCF, the first step is to make a solid Duran fibre and explore the behaviour of the glass during drawing conditions. Additionally, a solid fibre of 160 µm OD is used to obtain the loss transmission of the material itself and enables a comparison of the microstructured fibre (such as HCF) loss relative to the solid fibre. This comparison helps to identify the loss of HCF caused by confinement and by the additional steps to make the HCF. Note these fibres are made in house by Prof. Heike Ebendorff-Heidepriem, Dr. Erik Schartner and Dr. Georgios Tsiminis.

The Raman spectra of various glass materials such as Silica, F2, Duran, BK7, Ge and Te were also investigated.

5.2 – Experimental Method and Apparatus

As described in Chapter 2, light experiences attenuation as it travels along the fibre. Generally, fibres are used at near infrared (NIR) wavelengths due to the minimal attenuation in this spectral region (see Figure 3). However, the UV-VIS-IR attenuation spectrum does vary with glass type [25]. Therefore, to characterise transmission spectra in the UV-VIS-IR spectral window, a white light source (WLS) is used.

Attenuation through optical fibre is expressed by the total loss of optical power as a result of the various loss mechanisms [17, 24, 25] mentioned in Chapter 2. One of the techniques used to measure the transmission loss in the fibre is known as the cut–back technique. This technique requires that the transmission spectrum of a test fibre of known length L be iteratively measured and cut back into increasingly shorter pieces of the fibre. This technique has the advantage of reducing the effect of systematic coupling losses and canceling out Fresnel & coupling losses. Two types of light sources were used for cut–back measurements: narrowband and broadband. Firstly, spot loss measurements were conducted using a narrowband laser at 633nm (HeNe) as

a light source and a power meter for measuring power of the transmitted light at the fibre output (Figure 22a). Secondly, broadband loss measurements were conducted using a broadband light source and an optical spectrum analyzer (OSA) AQ-6315E for measuring output power at different wavelengths (see Figure 22b). Different microscope objectives (MO) were used, the magnification that provided the best light coupling efficiency into the fibre was selected. Efficient coupling into the fibre was achieved by controlling the fibre position using a 3D translation stage until the fibre tip reached the focal point of the objective, when the output power is maximised. Once the maximum of the optical power coupled is reached, the OSA is set up to scan from 350nm to 1750nm (valid for broadband loss). Note, when light is coupled into the fibre, no special attention was paid to excite a particular mode in the fibre. The first measurement was conducted, and the reading was imported into the loss measurement program. Subsequent cut-back measurements were repeated iteratively after cleaving the fibre by 1m intervals using FK11 cleaver (used only for solid fibre).

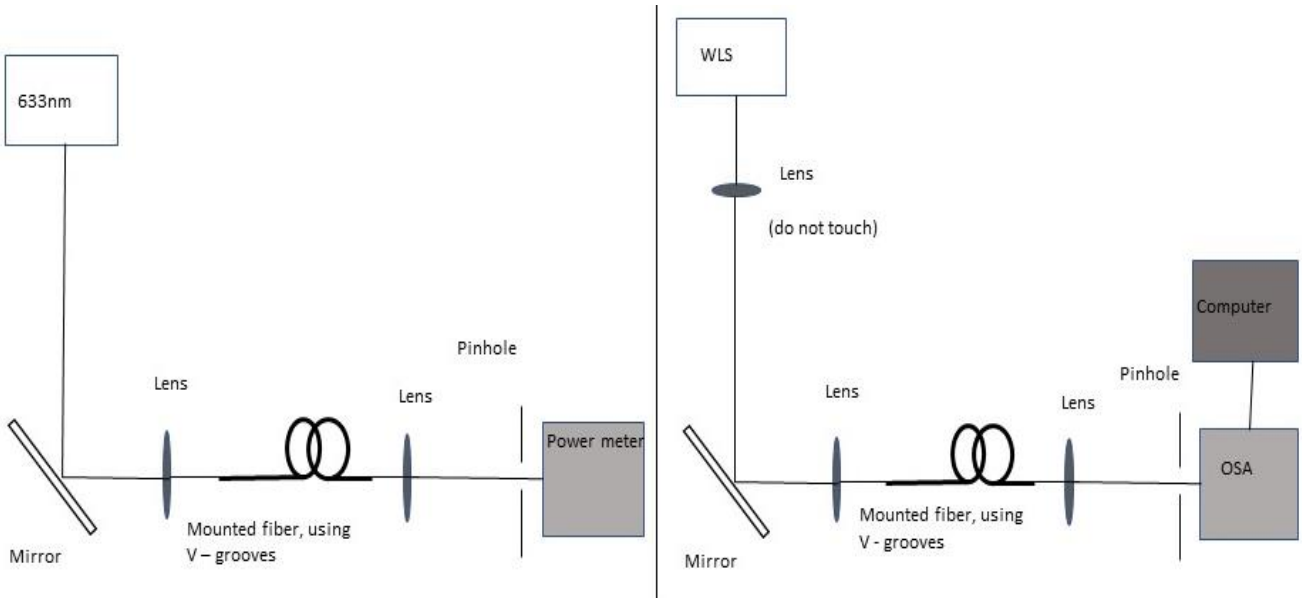

a *b*

Figure 22. Experimental setup for loss measurements using a) narrowband source and b) broadband source.

5.3 – Loss Measurement Results

5.3.1 – Solid Fibre

The broadband loss measurements of solid fibres made of F2 and Duran glass was conducted. The initial length of the fibre used for loss measurements was about 5 meters for both F2 and Duran glass. The end of the fibre was fitted into a fibre adapter connected directly to the

OSA. After the OSA was set up to read at one wavelength (for example, at 1 µm), the tip of the fibre where light was coupled via a 60X MO was adjusted to optimize coupling efficiency as described earlier.

As shown in Figure 23, the loss of the F2 solid fibre (red line) is under 2.9 dB/m between 490-550nm. Beyond 550nm, the loss of the F2 solid fibre continues to decrease and reaches 2.0dB/m at 640nm. The F2 solid fibre tested in this work has higher loss than previously reported loss, which is <1dB/m [67], and higher than F2 bulk glass, due to the lower quality of the fibre; the preform from which the F2 solid fibre tested here was made possibly contained bubbles and other imperfections trapped in the drawn fibre [68]. This could be the reason for the higher VIS-NIR loss in the F2 solid fibre tested in this work. The loss of the Duran solid fibre, which is under 9.5 dB/m between 490-640nm, represented by a black line in Figure 23, agrees with spot loss measurements within error which is represented by green dot (see Figure 23). However, the measured loss of the Duran solid fibre beyond 640nm becomes very noisy and is not represented in the figure.

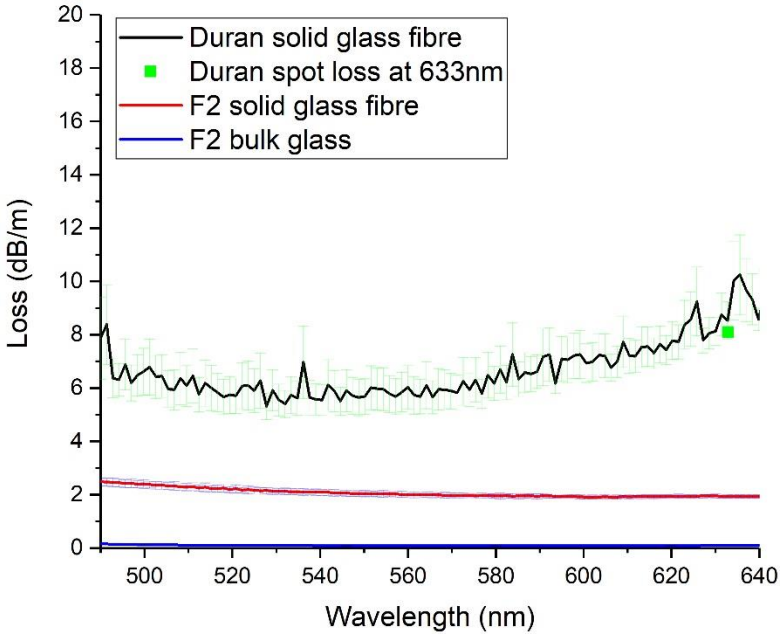

Figure 23. Loss of Duran solid fibre in black, Duran solid fibre spot loss at 633nm in green, loss of the F2 solid fibre glass in red, and loss of F2 bulk glass in blue.

5.3.2 – Hollow Core Fibre (HCF)

In this thesis, several HCFs were produced using different extruded preforms made of the F2 glass material. Figure 24 shows the cross-sectional image of the in-house made HCF – 1 made of F2 glass.

In this section, details of the loss measurement procedure and results are described. The spot loss measurements and broadband loss measurements were conducted for HCFs. A piece of fibre about 35-40 cm long was cleaved using a ceramic blade. As per Figure 22, the HCF was mounted onto the grooved stages using holding magnets with rubber underneath to avoid damaging the fibre. Light was coupled into the HCF fibre using a 20X MO lens due to its enhanced coupling efficiency compared to other lenses such as 100X, 60X or 40X. Output light passes through a 10X MO lens to collimate the beam. The output optical power was measured using a power meter and OSA, respectively.

To measure only the light that travels through the hollow core, a pinhole was used which blocks the light travelling in the fibre inner ring walls. After this first reading, about 5cm of the fibre is cleaved. The stage, together with the power meter or OSA, was shifted to keep the distance between the detector and the output light fixed.

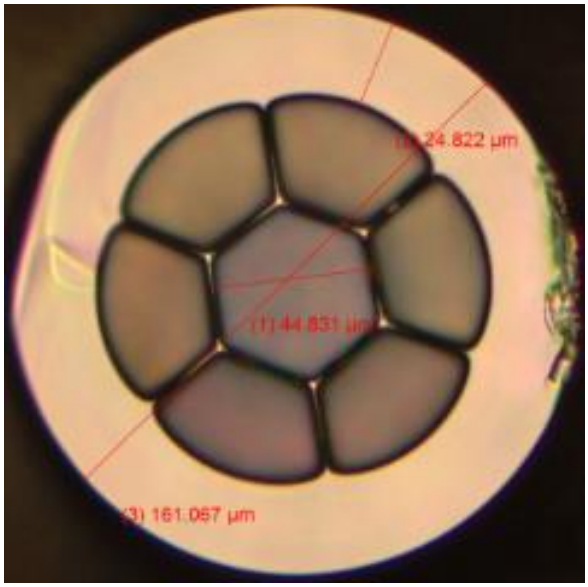

Figure 24. The cross-sectional image of the HCF made of F2 glass.

Broadband loss measurements were performed using WLS at visible spectrum of this in-house HCF. In this test, 4 different pieces of fibre named *a*, *b*, *c*, and *d*, each with length 40cm, were tested. The loss of the HCF – 1 varies between 20-60 dB/m in the visible spectrum as shown in Figure 25. A spot loss measurement at 633 nm was also performed, which shows a loss over 70 dB/m labelled as *e* and represented by a black square (see Figure 25).

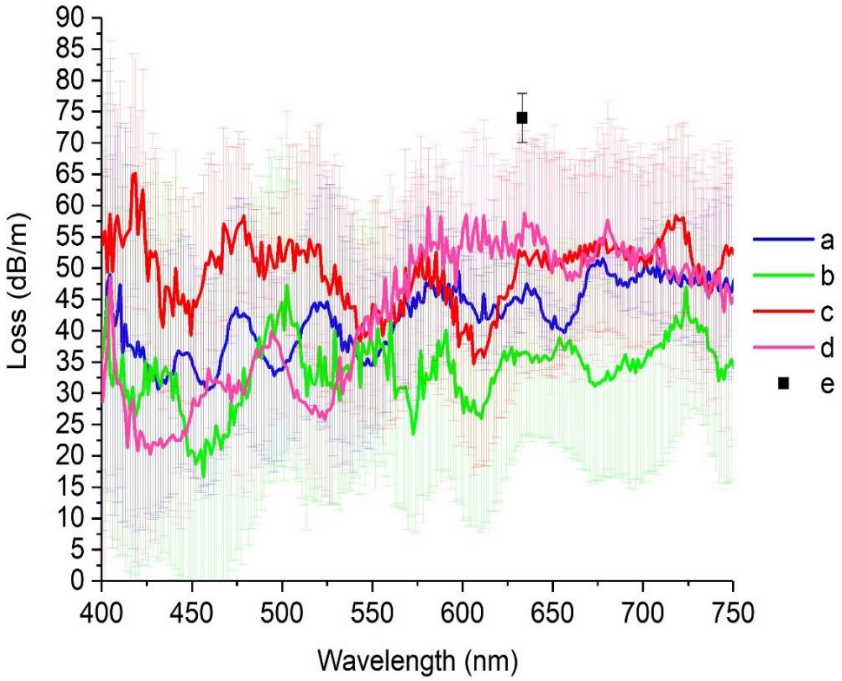

Figure 25. Broadband and spot loss of the HCF – 1 fibre made of F2 glass represented in red, blue, green, pink lines and black square respectively.

Figure 26 shows a loss of 20 dB/m near 420 nm and 700 nm, and over 100 dB/m near 600 nm of HCF – 2. The results obtained from a spot loss measurement at 633 nm shows a loss of 45 dB/m represented by the red square.

The loss measured for the fibre shown in Figure 26 (HCF – 2) is lower than the loss of HCF – 1 shown in Figure 25 at the same wavelength such as 420nm and 700nm, however, has higher loss at region between 600 to 650nm. This indicates that the inner structure geometry is not consistent between the fabrication of either set of fibres. In both cases, coupling the light into the fibre core was one of the biggest challenges due to major difficulties in the cleaving process of the fibre. The discrepancy between spot loss measurements and broadband loss measurements in both results shown in Figure 25 and Figure 26 is due to the variability of the HCFs.

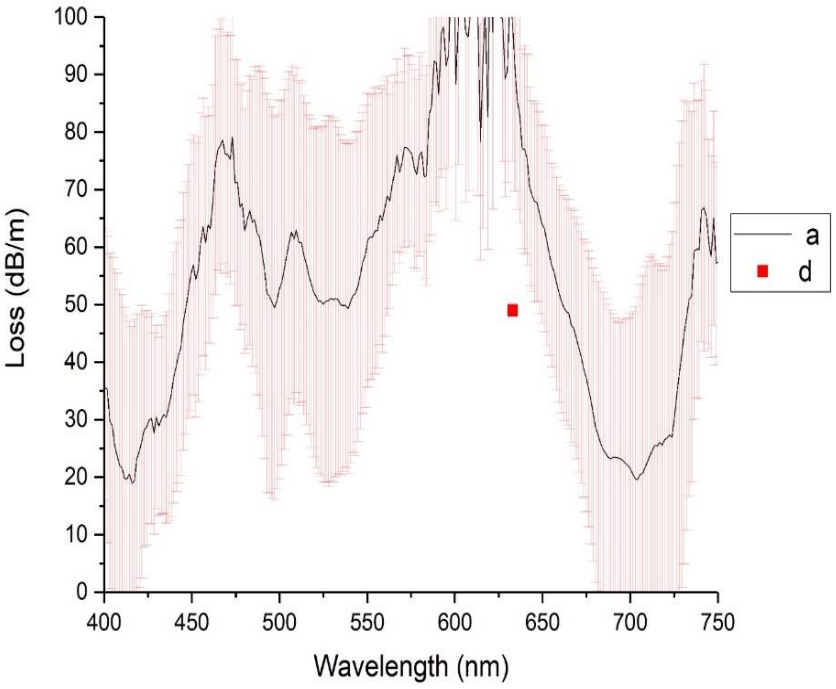

Figure 26. Broadband and spot loss of the HCF – 2 fibre made of F2 glass represented in black line and red square respectively.

5.4 – Glass Raman Background Signal

In recent years there has been great interest in using Raman spectroscopy to detect and analyse tissues and living cells [69, 70]. Raman spectroscopy has been demonstrated to be a suitable and useful technique, which utilises inelastic scattering to provide information about vibrational or rotational modes of molecular bonds [69, 71, 72]. Each chemical component in a sample has a unique molecular structure, so the sample's composition can be examined through analysis of the generated Raman signal [6, 33].

Each glass type has specific Raman bands based on their chemical composition and structure, which helps to identify them. However, this background Raman signal interferes with Raman measurements of molecular/tissue samples. The necessity to reduce the glass Raman signal generated in the glass core of the optical fibre motivates this experimental work. In order to overcome this issue, it is important to conduct Raman signal tests for different types of glass material, which could provide valuable information for future Raman detection research. In this experimental work, Raman signals are measured for Duran, Silica F300, BK7, F2 and Ge glass.

A single wavelength light source of 532nm is used for sample excitation. Choice of wavelength for glass Raman scanning is based on Raman scattering strength which is proportional to the fourth power of the excitation frequency v^4. This means higher frequencies are able to generate stronger Raman signals. However, the disadvantage of using higher frequencies is that the glass, and often organic samples, generate high autofluorescence background signals due to emission

of light by sample when they have absorbed light. Furthermore, higher frequencies can easily damage biological samples. Therefore, using 532nm is considered a suitable balance which would not damage a biological sample for optical powers under 30mW, while still delivering strong Raman spectra.

The glass Raman signal for various glasses was measured to determine the position and intensity of the Raman signal. This enables crucial information on how Raman signals overlap with Raman signals of tissues or chemicals of interest. Table 11 shows some of the interest Raman signals.

Table 11. Different cases of tissue identification using Raman spectroscopy.

Cases where Raman spectroscopy is used	Wavenumber in (1/cm)
Fat, muscle esophagus, brain, aorta, skin, normal breast tissue, malignant breast tumor	800 - 1800
Brain tissue, metastases malignant	2700-3550
Cyclohexane	500-4000
Cholesterol ester	2700-3000

A billet of the same size and geometry (30mm thickness) of the glass was used for measurements. The excitation light was aligned using two mirrors and a notch filter as shown in Figure 27. The excited Raman signal was collected using an optical fibre, and the collected data was processed using the following formula:

$$\Delta\omega = \left(\frac{1}{\lambda} - \frac{1}{\lambda_1}\right), \qquad 5.1$$

where $\Delta\omega$ is the Raman shift expressed in wavenumber, λ_1 is the Raman spectrum wavelength, λ is the excitation wavelength.

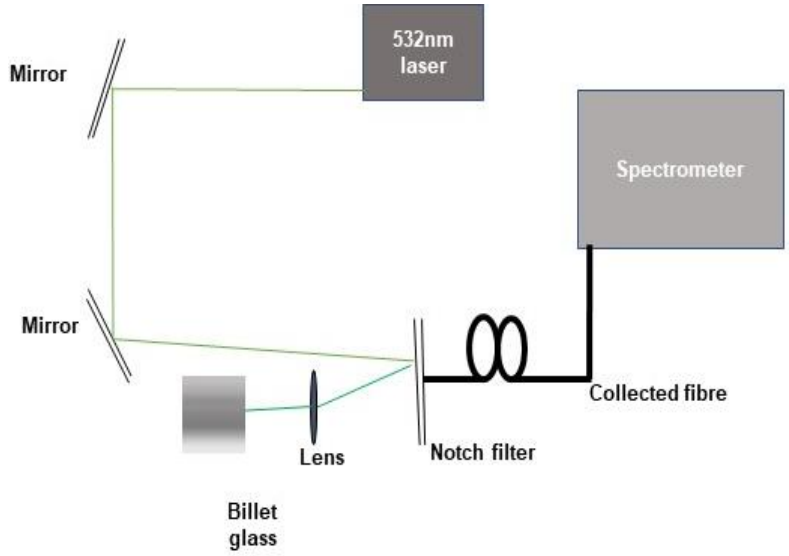

Figure 27. Experimental setup for Raman measurements.

Figure 28 shows that the region of interest for Raman detection overlaps with the Raman background signals of the five glass types tested. It can be seen that the Raman signal for Duran is lower than for BK7 glass and is less broad than BK7 from 400 – 1200 cm^{-1}. F2 glass has a very strong Raman background signal with peaks of 11000 – 13000 counts between 350 – 450 cm^{-1} and 950 – 1070 cm^{-1}, which would obstruct Raman detection in this range.

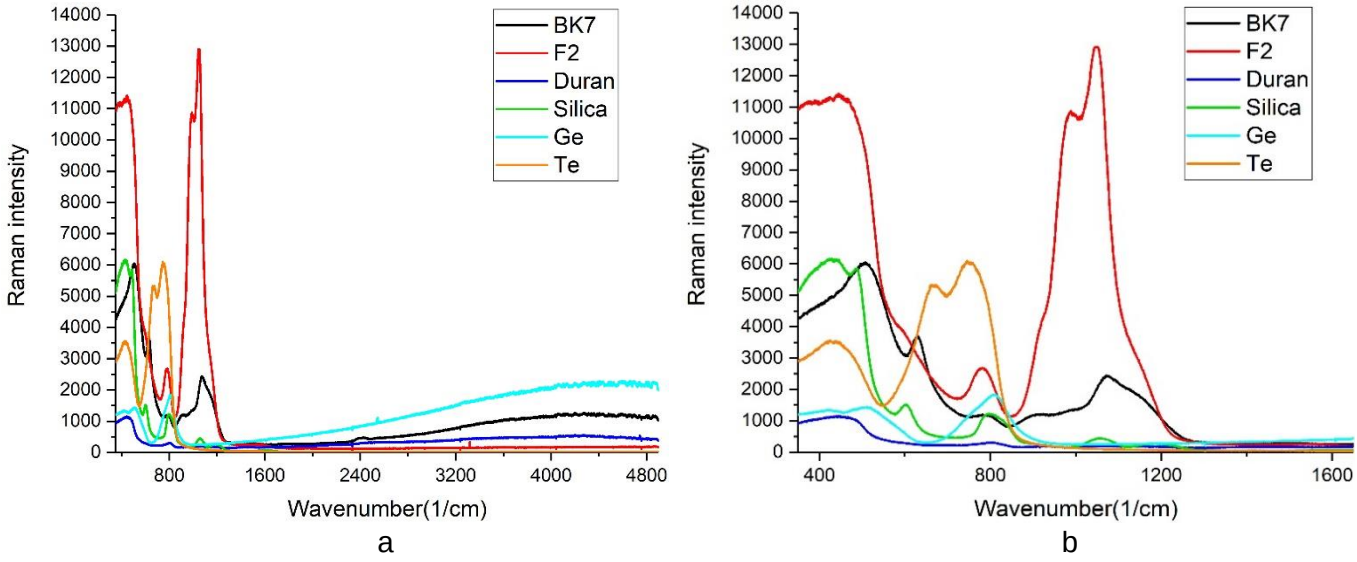

Figure 28. Raman signal of Silica, F2, BK, Duran, Ge and Te glass material, a) 400 – 4800 wavenumber and b) 400 – 1600 wavenumber range.

5.5 – Discussion

The optical loss of a glass material is one of the most important parameters for glass optical fibres. As can be seen from the measurements in this chapter, Duran glass material has higher loss compared to F2 glass (as shown in Figure 23) and the loss increases with increasing wavelength. In Figure 23, similar results were presented between F2 solid fibre glass and F2 bulk glass material, where F2 solid fibre glass has higher loss than F2 bulk glass material, possibly due to imperfections in the F2 solid fibre. The loss of bands (pieces) of the HCF – 1 made of F2 glass shown in Figure 25 were high due to variations and coupling efficiency. Note that, in the future, a loss comparison between the Duran glass fibre and Duran bulk glass is needed.

It is worth noting some limitations of F2 glass with Raman spectroscopy. As per the result shown in Figure 28, F2 glass fibre has a strong Raman signal in the range between 350 – 450 cm^{-1} and 950 – 1070 cm^{-1}. The Duran glass material shows high fluorescence in the range between 1000 – 4900 cm^{-1} compared to F2 glass material. Considering the time limitation in this project, the Raman glass signal will be the study of future investigation.

Chapter 6 – Conclusion

The overall aim of this thesis was to investigate the effect of glass composition, fibre structure and aging on the mechanical properties of Young's modulus, Weibull distribution, characteristic strength, and Weibull slope. Additionally, the impact of the inner structure geometry and glass type on optical losses was investigated. In this work, the statistical Weibull distribution was used to examine the reliability of the solid glass optical fibre made of different materials as well as structured optical fibres, when these fibres are subjected to a pulling force. General conclusions from this work are as follows.

1. Results indicate that the strength of the solid glass fibres is consistent with Young's modulus values. The characteristic strength of the solid fibres decreases with decreasing Young's modulus values, with one exception: F2 solid fibre shows a surprisingly high characteristic strength for its relatively low Young's modulus compare to LWQ, Duran and Ge solid glass fibre. Additionally, aging effects in soft glass such as F2 seem to be insignificant as demonstrated by the insensitivity of the F2 solid glass fibre (see characteristic strength of both sub-populations of all the F2s in Table 7). Furthermore, the inflation ratio of capillary fibres reduces fibre strength in general and decreases the Weibull slope (reliability) of the fibre compared with standard SMF28(F300) fibre. The suspended core fibre (SCF) shows reduced fibre strength, but its reliability is high compared to SMF28(F300) fibre. The results shown here indicate that the strength of the fibre with one hole (capillary fibre) does not change significantly from the strength of the SCF (fibre with three holes).

2. Duran glass material has higher transmission loss compared to F2 glass, especially in the range 600 nm and above, where the signal is strongly attenuated. Additionally, HCFs made of F2 glass material are shown to have very high loss compared to F2 solid fibre. For example, the loss of F2 glass drops below 2 dB/m beyond 640nm, but the loss of HCF in that same range varies between 20 to over 60 dB/m in both fibres tested, which might be related to the fibre structure. Also, coupling light into HCFs is one of the main difficulties due to the cleaving process.

The work presented here has generated crucial insights for both the mechanical and optical features of the glass materials used for optical fibre and fibre structures including HCF. In the future, major work would be required to investigate and optimise both the mechanical stability of the optical fibres and the use of HCFs with low transmission loss, which is key to application in biomedical sensing.

Appendixes A

Statistical analysis of the collected data to generate Weibull distribution of SMF28(F300) fibre

N –*total fibre tested*	*Ascending order of fibre failure* **i**	Fibre Stress to failure *σ (GPa)*	Median rank $P = \frac{i - 0.3}{N + 0.4}$	***Ln (σ (GPa))***	***Ln (Ln(1/1-F))***
20	1	0.47362	0.03431	-0.74735	-3.3548
	2	0.4755	0.08333	-0.74339	-2.44172
	3	0.48073	0.13235	-0.73244	-1.95214
	4	0.50395	0.18137	-0.68527	-1.60881
	5	0.55213	0.23039	-0.59396	-1.33989
	6	0.5567	0.27941	-0.58573	-1.1157
	7	0.56126	0.32843	-0.57757	-0.92095
	8	0.60501	0.37745	-0.50251	-0.74669
	9	0.60649	0.42647	-0.50007	-0.58708
	10	0.65292	0.47549	-0.42629	-0.43805
	11	0.65507	0.52451	-0.42301	-0.29651
	12	0.67614	0.57353	-0.39135	-0.15992
	13	0.68446	0.62255	-0.37912	-0.02602
	14	0.71936	0.67157	-0.3294	0.10744
	15	0.72285	0.72059	-0.32456	0.243
	16	0.72379	0.76961	-0.32326	0.38388
	17	0.75694	0.81863	-0.27848	0.53486
	18	0.80136	0.86765	-0.22145	0.70423
	19	0.84176	0.91667	-0.17227	0.91024
	20	0.85276	0.96569	-0.15928	1.21557

Appendixes B

The glass optical fibre types, their dimesions, fabrication technique and in house code.

Fibre structure	Glass material type	Code	OD (um)	ID (um)	In house code	Fabrication technique
Solid fibre	Fused Silica	SMF28(F300)	125		SMF28	Commercially avalable, made of F300
	Quartz Silica	LWQ	125		LWQ	Drawn into fibre from commercial rod
	Borosilicate	Duran	160		Duran	Drawn into fibre from commercial rod
	Lead silicate	F2a	160		F2F355	Drawn into fibre from commerical rod
	Lead silicate	F2b	160		F2F342	Drawn into fibre from extruded rod preform made of commercial rod
	Lead silicate	F2c	160		F2F296	Drawn into fibre from extruded rod preform made of commercial rod
	Lead silicate	F2d	160		F2F231	Drawn into fibre from extruded rod preform made of commercial rod
	Germanate	Ge	160		Ge	Drawn into fibre from extruded rod preform
	Tellurite	Te	160		Te	Drawn into fibre from extruded rod preform
	Fluoride	ZBLAN	160		ZBLAN	Drawn into fibre from extruded rod preform
Suspended core (three hole)	Quarzt Silica	LWQ-SCF	160		LWQ-WW	Drawn into fibre from in-house preform made from commercial rod
	Fused Silica	F300-SCF	160		ES14 WW	Drawn into fibre from in-house preform made from commercial rod
Capillary (single hole)	Fused Silica	F300-C1	125	36	ES27	Drawn into fibre from commercial capillary preform
	Fused Silica	F300-C2	125	40	ES27	Drawn into fibre from commercial capillary preform
	Fused Silica	F300-C3	125	56	ES27	Drawn into fibre from commercial capillary preform
	Fused Silica	F300-C4	125	66	ES27	Drawn into fibre from commercial capillary preform
	Fused Silica	F300-C5	125	75	ES27	Drawn into fibre from commercial capillary preform

References

1. Antunes, P., et al., *Mechanical properties of optical fibers*, in *Selected Topics on Optical Fiber Technology*. 2012, InTech.
2. Antunes, P., et al., *Mechanical properties of optical fibers*.
3. Ebendorff-Heidepriem, H. and T.M. Monro, *Extrusion of complex preforms for microstructured optical fibers.* Optics Express, 2007. **15**(23): p. 15086-15092.
4. Monro, T.M., et al., *Sensing with microstructured optical fibres.* Measurement Science and Technology, 2001. **12**(7): p. 854.
5. Brown, W.G., et al. *Optical fibres in biomedical applications: Effect of a biological medium on static fatigue*. in *Optical Fibre Technology (ACOFT), 2010 35th Australian Conference on*. 2010. IEEE.
6. Motz, J.T., et al., *Optical fiber probe for biomedical Raman spectroscopy.* Applied optics, 2004. **43**(3): p. 542-554.
7. Schartner, E.P., *Hydrogen peroxide sensing with microstructured optical fibres: fuel, wine & babies*. 2012.
8. Matthewson, M.J. *Optical fiber reliability models*. in *Fiber Optics Reliability and Testing: A Critical Review*. 1993. International Society for Optics and Photonics.
9. MATTHEWSON, M. and C.R. Kurkjian, *Environmental effects on the static fatigue of silica optical fiber.* Journal of the American Ceramic Society, 1988. **71**(3): p. 177-183.
10. Krafft, C. and V. Sergo, *Biomedical applications of Raman and infrared spectroscopy to diagnose tissues.* Journal of Spectroscopy, 2006. **20**(5-6): p. 195-218.
11. Quinn, J.B. and G.D. Quinn, *A practical and systematic review of Weibull statistics for reporting strengths of dental materials.* Dental Materials, 2010. **26**(2): p. 135-147.
12. Miao, P., et al., *Mechanical reliability of optical fibre sensors and SmartRods for tunnel displacement monitoring.* Smart Materials and Structures, 2007. **16**(2): p. 382.
13. Andersons, J., et al., *Glass fibre strength distribution determined by common experimental methods.* Composites Science and Technology, 2002. **62**(1): p. 131-145.
14. Ebendorff-Heidepriem, H. and T.M. Monro, *Analysis of glass flow during extrusion of optical fiber preforms.* Optical Materials Express, 2012. **2**(3): p. 304-320.
15. Furukawa, T., S.A. Brawer, and W.B. White, *The structure of lead silicate glasses determined by vibrational spectroscopy.* Journal of Materials Science, 1978. **13**(2): p. 268-282.
16. Tsiminis, G., et al., *Single-ring hollow core optical fibers made by glass billet extrusion for Raman sensing.* Optics Express, 2016. **24**(6): p. 5911-5917.
17. Fang, Z., et al., *Fundamentals of optical fiber sensors*. Vol. 226. 2012: John Wiley & Sons.
18. France, P., *Fluoride glass optical fibres*. 2012: Springer Science & Business Media.
19. Bahaa, E.S. and C.T. Malvin, *Fundamentals of photonics.* New York/A WILEY-INTERSCIENCE PUBLICATION, 1991.
20. Schartner, E.P., et al., *Taming the light in microstructured optical fibers for sensing.* International Journal of Applied Glass Science, 2015. **6**(3): p. 229-239.
21. Tsiminis, G., et al. *Extruded single ring hollow core optical fibers for Raman sensing*. in *23rd International Conference on Optical Fibre Sensors*. 2014. International Society for Optics and Photonics.
22. Snyder, A.W. and J. Love, *Optical waveguide theory*. 2012: Springer Science & Business Media.
23. Hecht, E., *Optics, 4th.* International edition, Addison-Wesley, San Francisco, 2002. **3**: p. 2.
24. Okamoto, K., *Fundamentals of optical waveguides*. 2006: Academic press.
25. Bailey, D. and E. Wright, *Practical fiber optics*. 2003: Elsevier.
26. Kalish, D., et al., *Fiber characterization-mechanical.* Optical fiber telecommunications, 1979: p. 401-434.

27. Issa, N.A. and L. Poladian, *Vector wave expansion method for leaky modes of microstructured optical fibers.* Journal of Lightwave Technology, 2003. **21**(4): p. 1005-1012.
28. Newport, https://www.newport.com/t/fiber-optic-basics, Fiber Optic Basics.
29. Monro, T.M. and H. Ebendorff-Heidepriem, *Progress in microstructured optical fibers.* Annu. Rev. Mater. Res., 2006. **36**: p. 467-495.
30. Cregan, R., et al., *Single-mode photonic band gap guidance of light in air.* science, 1999. **285**(5433): p. 1537-1539.
31. Belardi, W. and J.C. Knight, *Hollow antiresonant fibers with reduced attenuation.* Optics letters, 2014. **39**(7): p. 1853-1856.
32. Tsiminis, G., et al., *Single-ring hollow core optical fibers made by glass billet extrusion for Raman sensing.* Optics express, 2016. **24**(6): p. 5911-5917.
33. Tsiminis, G., et al. *Hollow-Core Optical Fibers Made by Glass Billet Extrusion as Sensors for Raman Spectroscopy*. in *Australian Conference on Optical Fibre Technology*. 2016. Optical Society of America.
34. *Fiber Fabrication.* https://www.rp-photonics.com/fiber_fabrication.html.
35. Monro, T.M. and H. Ebendorff-Heidepriem, *Progress in Microstructured Optical Fibers.* Annual Review of Materials Research, 2006. **36**(1): p. 467-495.
36. Kapur andL, K. and R. Lamberson, *Reliability in Engineering Design. New York: John Willey & Sons*. 1977, Inc.
37. Symposium on Photonics, M. and Devices, *Advances in photonic materials and devices proceedings of the 106th Annual Meeting of the American Ceramic Society : Indianapolis, Indiana, USA (2004)*. Photonics materials and devices, ed. S. Bhandarkar and I. American Ceramic Society. Meeting : Indianapolis. 2005, Westerville, Ohio: American Ceramic Society.
38. Schartner, E.P., A. Dowler, and H. Ebendorff-Heidepriem, *Fabrication of low-loss, small-core exposed core microstructured optical fibers.* Optical Materials Express, 2017. **7**(5): p. 1496-1502.
39. Roeder, E., *Extrusion of glass.* Journal of Non-Crystalline Solids, 1971. **5**(5): p. 377-388.
40. Wachtman, J.B., W.R. Cannon, and M.J. Matthewson, *Mechanical properties of ceramics*. 2009: John Wiley & Sons.
41. Roylance, D., *Mechanical properties of materials.* Massachusetts Institute of Technology, 2008: p. 51-78.
42. Sonnenfeld, C., et al., *Mechanical Strength of Microstructured Optical Fibers.* Journal of Lightwave Technology, 2014. **32**(12): p. 2193-2201.
43. Matthewson, M.J., *Optical fiber mechanical testing techniques.* 1993. **10272**: p. 1027205.
44. Korwin-Edson, M.L., D.A. Hofmann, and P.B. McGinnis, *Strength of high performance glass reinforcement fiber.* International Journal of Applied Glass Science, 2012. **3**(2): p. 107-121.
45. Le Bourhis, E., *Glass: mechanics and technology*. 2008: John Wiley & Sons.
46. Salamin, E., *The Weibull distribution in the strength of glass.* graduate class assignment: Opti. **521**.
47. Glaesemann, D.G.S., *Optical Fiber Mechanical Reliability.* (July 2017).
48. Helfinstine, J.D. and F. Quan, *Optical fibre strength/fatigue experiments.* Optics & Laser Technology, 1982. **14**(3): p. 133-136.
49. Kurkjian, C.R., J.T. Krause, and M.J. Matthewson, *Strength and fatigue of silica optical fibers.* Journal of Lightwave Technology, 1989. **7**(9): p. 1360-1370.
50. El Abdi, R., et al., *New method for strength improvement of silica optical fibers.* Optics and Lasers in Engineering, 2008. **46**(3): p. 222-229.
51. Kececioglu, D., *Reliability engineering handbook*. Vol. 1. 2002: DEStech Publications, Inc.
52. Abernethy, R.B., et al., *Weibull analysis handbook*. 1983, Pratt and Whitney West Palm beach fl Government Products DIV.
53. R. V. CURTIS, A.S.J., *Analysis of strength data using two- and three-parameter Weibull models.* JOURNAL OF MATERIALS SCIENCE (1998). **33**(1151—1157).

54. F. Pigeon, S.P., A. Mure-Ravaud, H. Gagnaire and C. Veillas, *OPTICAL FIBRE YOUNG MODULUS MEASUREMENT USING AN OPTICAL METHOD.* ELECTRONICS LE77ERS 21sr May 1992 **Vol. 28**(No. 11).
55. Xu, Z., *Comparing graphical method and a modified method to fit weibull distribution.* 2012.
56. Bourahli, M., *Uni-and bimodal Weibull distribution for analyzing the tensile strength of Diss fibers.* Journal of natural fibers, 2018. **15**(6): p. 843-852.
57. Ingman, D., T. Mirer, and E. Suhir, *Dynamic Physical Reliability in Application to Photonic Materials*, in *Micro-and Opto-Electronic Materials and Structures: Physics, Mechanics, Design, Reliability, Packaging*. 2007, Springer. p. A571-A594.
58. Gupta, V., *Melt-spinning processes Manufactured Fibre Technology ed VB Gupta and VK Kothari*. 1997, Berlin: Springer.
59. Volf, M.B., *Technical approach to glass*. 1990.
60. Schott, A., *Mainz (Germany): Optical Glass Catalog.* Available for download at www. schott. com/ advanced_ optics/ english/ download/ schott-optical-glass-collection-datasheets-july-2015-eng. pdf.
61. Bayya, S.S., et al., *Germanate glass as a window for high energy laser systems.* Optics Express, 2006. **14**(24): p. 11687-11693.
62. Delben, A., et al., *Mechanical properties of ZBLAN glasses.* Journal of non-crystalline solids, 1993. **161**: p. 165-168.
63. Inaba, S., S. Fujino, and K. Morinaga, *Young's modulus and compositional parameters of oxide glasses.* Journal of the American Ceramic Society, 1999. **82**(12): p. 3501-3507.
64. Kostecki, R., et al., *Predicting the drawing conditions for microstructured optical fiber fabrication.* Optical Materials Express, 2014. **4**(1): p. 29-40.
65. Shengling, W., et al., *Effects of pressurization and surface tension on drawing Ge-Sb-Se chalcogenide glass suspended-core fiber.* Optical Materials Express, 2019. **9**(4): p. 1933-1944.
66. Doronina-Amitonova, L.V., et al., *Raman detection of cell proliferation probes with antiresonance-guiding hollow fibers.* Optics letters, 2012. **37**(22): p. 4642-4644.
67. Ebendorff-Heidepriem, H., Y. Li, and T.M. Monro. *Reduced loss in extruded soft glass microstructured fibre*. in *COIN-ACOFT 2007-Joint International Conference on the Optical Internet and the 32nd Australian Conference on Optical Fibre Technology*. 2007. IEEE.
68. Carter, S., et al. *Extrinsic Scatter Losses in ZrF4-Based Infrared Fibres*. in *Materials Science Forum*. 1985. Trans Tech Publ.
69. Shim, M.G., et al., *Study of fiber-optic probes for in vivo medical Raman spectroscopy.* Applied Spectroscopy, 1999. **53**(6): p. 619-627.
70. Konorov, S.O., et al., *Hollow-core photonic crystal fiber-optic probes for Raman spectroscopy.* Optics letters, 2006. **31**(12): p. 1911-1913.
71. Hanlon, E.B., et al., *Prospects for in vivo Raman spectroscopy.* Physics in Medicine and Biology, 2000. **45**(2): p. R1-R59.
72. Krafft, C. and V. Sergo, *Biomedical applications of Raman and infrared spectroscopy to diagnose tissues.* Spectroscopy, 2006. **20**(5-6): p. 195-218.